

Correlated Components Analysis — Extracting Reliable Dimensions in Multivariate Data

Lucas C. Parra

PARRA@CCNY.CUNY.EDU

*Department of Biomedical Engineering
City University of New York
New York, NY 10031, USA*

Stefan Haufe

STEFAN.HAUFE@TU-BERLIN.DE

*Machine Learning Group
Technische Universität Berlin
10587 Berlin, Germany*

Jacek P. Dmochowski

JDMOCHOWSKI@CCNY.CUNY.EDU

*Department of Biomedical Engineering
City University of New York
New York, NY 10031, USA*

Abstract

How does one find data dimensions that are reliably expressed across repetitions? For example, in neuroscience one may want to identify combinations of brain signals that are reliably activated across multiple trials or subjects. For a clinical assessment with multiple ratings, one may want to identify an aggregate score that is reliably reproduced across raters. The approach proposed here — “correlated components analysis” — is to identify components that maximally correlate between repetitions (e.g. trials, subjects, raters). This can be expressed as the maximization of the ratio of between-repetition to within-repetition covariance, resulting in a generalized eigenvalue problem. We show that covariances can be computed efficiently without explicitly considering all pairs of repetitions, that the result is equivalent to multi-class linear discriminant analysis for unbiased signals, and that the approach also maximizes reliability, defined as the mean divided by the deviation across repetitions. We also extend the method to non-linear components using kernels, discuss regularization to improve numerical stability, present parametric and non-parametric tests to establish statistical significance, and provide code.

1. Introduction

Consider the following scenario: A set of human subjects are shown a movie while the activity from their brain is recorded (Dmochowski et al., 2012). Guided by the assumption that the movie evokes similar brain responses in each subject, the goal is then to identify movie-related brain activity that is common across subjects. Because activity is distributed across multiple sensors, we would like to find linear combinations of sensors (that is, underlying *components*, or, factors) that have a similar time course in all subjects. In other words, we would like to identify components that have high *inter-subject correlation* (ISC).

In a different setting, the task may be to assess motor skills during child development. A clinician observes children at various tasks and provides a rating for each child and task

(Rousson et al., 2002). Typically, ratings are combined across tasks so that each child obtains a single aggregate performance score. But how should individual task ratings be combined? Traditionally, this is done by simple averaging of related scores. We propose instead a data-driven approach that aims to make the aggregate scores of different raters most consistent. This means that we want to combine scores so as to maximize *inter-rater reliability*.

What is common in these two examples is the goal of identifying directions in multi-variate data sets that are reliably reproduced across repetitions. Correlated Components Analysis (CorrCA) accomplishes this goal. CorrCA was originally developed in the context of neuroimaging studies to extract similar activity in multiple subjects (Dmochowski et al., 2012), and was re-developed independently to extract reliable brain responses across repeated trials in a single subject (Tanaka et al., 2013). We will discuss the utility of CorrCA for analyzing inter-subject correlations of brain signals, but also demonstrate how the technique can be used to identify aggregate ratings with high inter-rater reliability.

More generally, CorrCA is applicable whenever a data volume is available with dimensions $T \times D \times N$, where N are repetitions of some sort. The method then identifies dimensions in D -dimensional space such that the data projected onto these dimensions maximally correlates between N repeated measurements, with correlation measured across T samples. This is somewhat similar to Principal Component Analysis (PCA, Hotelling, 1933) in that CorrCA finds a set of D -dimensional component vectors that linearly decompose a data set (of size $D \times T$). Instead of capturing dimensions with maximum variance within a single data set as in PCA, here we capture the dimensions with maximum correlation between the N data sets. The optimality criterion of CorrCA is identical to that of Canonical Correlation Analysis (CCA, Hotelling, 1936), but the method differs in that a single set of linear projections is applied to all data sets, whereas CCA yields a different set of projection vectors for each data set, and is, therefore, also capable of dealing with heterogeneous data sources of different dimensionality. Conventional CCA operates on $N = 2$ data sets but has been generalized to the case of multiple data sets ($N > 2$, Kettenring, 1971), where in this multi-set CCA each data set has its own projection vector. Therefore, CorrCA can be seen as a constrained version of (multi-set) CCA, where each data set is projected into a common space.

In the present paper, we provide a formal characterization of CorrCA, which has been lacking in the previous, more applied literature. In particular, we show that maximizing the correlation across repeated measurements is indeed equivalent to maximizing the “reliability” of the projected data, defined here as the mean over repetitions, divided by the deviation from this mean. Note that this reliability metric is a type of signal-to-noise ratio (SNR), and finding components that maximize SNR leads to a joint-diagonalization problem (de Cheveigné and Parra, 2014) similar to what we will present here.

The present work also generalizes CorrCA to include non-linear feature mappings using the well-known kernel approach. The formulation largely follows the non-linear generalization of Linear Discriminant Analysis (LDA) using kernels (Lai and Fyfe, 2000). LDA is in particular important to the present work as we show that CorrCA, which maximizes the ratio of between- to within-repetition covariance gives the same result as LDA, which maximizes the between-class over the within-class variance.

Before we present the mathematical treatment, we begin with a simple two-dimensional example to visualize the basic concept of identifying common signal components that are contained in a shared linear dimension.

2. Extracting shared dimensions — an illustrative example

For this illustrative example we consider a simulation of electrical brain signals recorded from multiple subjects. Assume that we have two sensors, $x_1(t)$ and $x_2(t)$, which record signals over time from each of two subjects, as shown in Figure 1 A & B. The figure caption details the generation of the data; briefly, there are two “sources” of signal, one has a common waveform for both subjects, while a second source has a subject-dependent waveform. The common waveform induces a correlation between subjects in both sensors, although the exact waveform is not immediately apparent in the individual time courses (Figure 1 A & B). The source directions do become clear from a scatter plot of the same data (Figure 1 C, blue and red arrows). Here, for each time point t we have connected both subjects by line. Evidently, at any point in time, the signals of the two subjects lie somewhere along a line (in the direction of the uncommon source, blue arrow), but the lines are shifted in parallel (in direction of the common source, red arrow). The locations along the gray lines are determined by the subject-dependent waveform, while the magnitude of the shift is determined by the common waveform. Now let’s select a linear transformation, \mathbf{V} , to map this data onto a component space, $\mathbf{y}(t)$:

$$\mathbf{y}(t) = \mathbf{V}^\top \mathbf{x}(t), \quad (1)$$

such that the component signals are maximally correlated between subjects. With this choice, the time course for both subjects in the first component dimension, $y_1(t)$, are now perfectly correlated (Figure 1 D). Thus, we have extracted the common source of variation in these two subjects, whereas the second dimension, $y_2(t)$, now captures a waveform that is not common between subjects (Figure 1 E). As a result, the gray lines in the scatter plot are now vertical (Figure 1 F), separating the signal into reproducible (y_1) and non-reproducible dimensions (y_2). Evidently, with \mathbf{V} we have identified the source directions (blue and red arrow) from these paired measurements alone.

Correlated Component Analysis aims to identify the unknown projection matrix \mathbf{V} from the time course $\mathbf{x}(t)$ alone.

3. Problem statement: Maximal inter-subject correlation

The specific objective of CorrCA is to find dimensions in multivariate data that maximize correlation between repetitions. Denote the D -dimensional data with $\mathbf{x}_i^l \in \mathbb{R}^D$, where $i = 1, \dots, T$ enumerates exemplars in a sample, and $l = 1, \dots, N$ represents repeated renditions of this sample. In the case of brain signals, the exemplars represent time points, so that i indexes a time sequence of length T , and l indexes N repeated recordings (subjects or trials). In the case of a clinical assessment instrument, i may index individuals receiving a rating, while l indexes multiple raters, or repeated ratings given to the same individuals by a single rater. In both instances, the observations are D -dimensional (D sensors that record brain signals, or D items rated in the assessment instrument). For simplicity, in

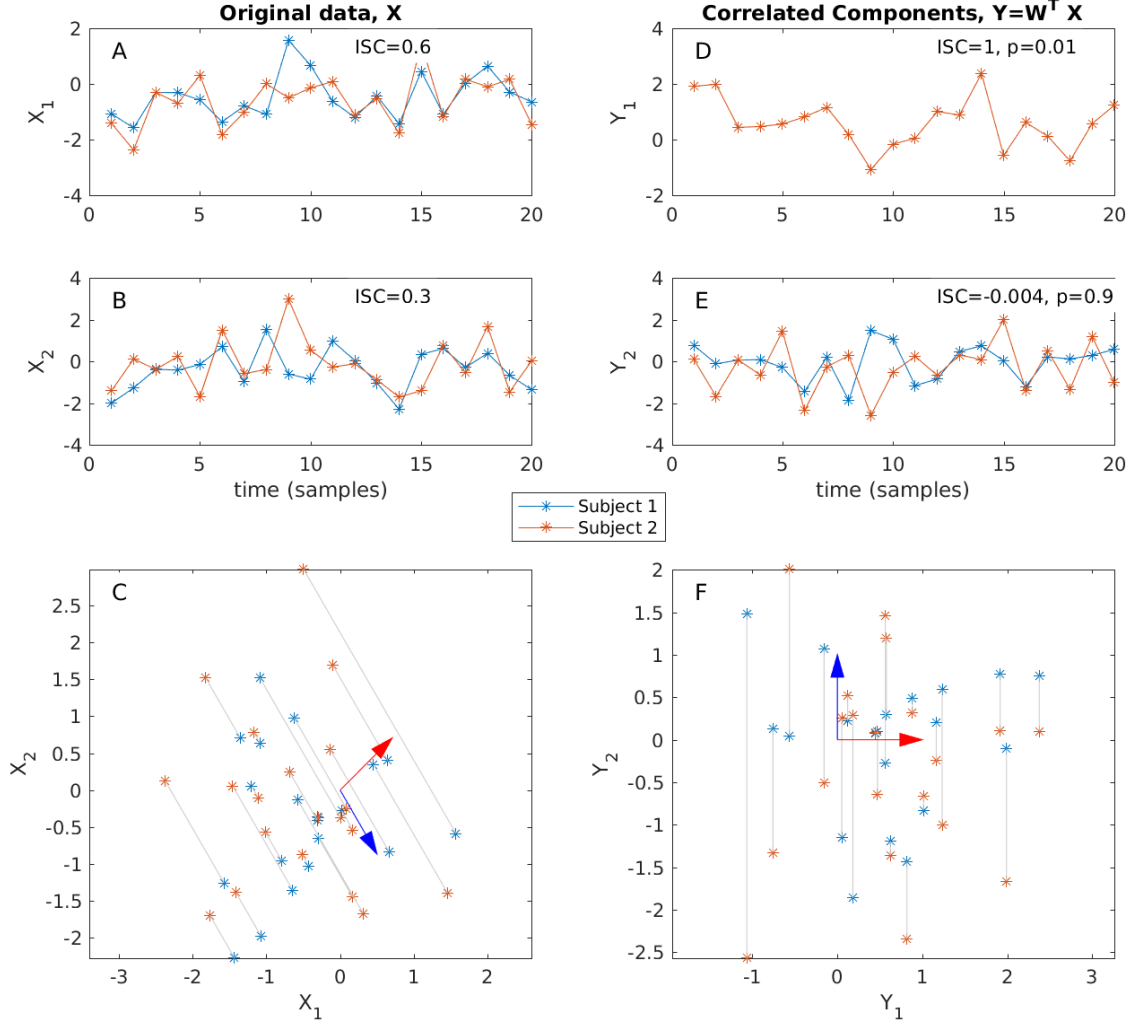


Figure 1: **Extraction of a correlated component in 2D time courses.** A common electrical current source, $s(t)$, is captured by voltage sensors $x_{1l}(t)$ and $x_{2l}(t)$ for subject l . This common source contributes with identical scaling a and b for both subjects: $x_{1l}(t) = as(t) + c\xi_l(t)$, $x_{2l}(t) = bs(t) + d\xi_l(t)$, where $\xi_l(t)$ is a source that contributes with a different value to each subject l but with the same coefficients c, d . Note that current sources contribute additively to a voltage recording in a resistive medium, hence the addition. (A) Time courses $x_{1l}(t)$ for both subjects. (B) Time courses $x_{2l}(t)$ (C) Same data, but now individual time points are connected (by gray line) between the subjects. The sources directions $[a, b]$ and $[c, d]$ are indicated with a red and blue arrow respectively and are the same for both subjects, i.e. they are “shared” dimensions. (D) Projection $y_{1l}(t)$ with maximal correlation. The time courses of the two subjects are perfectly correlated with inter-subject correlation, $\text{ISC}=1$. (E) Projection $y_{2l}(t)$ that is not common between subjects. (F) Along dimension y_1 , both subjects’ data are expressed identically, i.e. this is the (“reliable”) source dimension that is shared between the two subjects. Values along dimension y_2 differ randomly between subjects. This dimension is not “reliable” across subjects.

the following we will stick with the terminology of time and subjects, so that correlation is measured between subjects and across time. When necessary, we will rephrase the resulting expressions for the case of assessing inter-rater correlation or test-retest correlation.

The goal is now to identify a linear combination of these D measures, defined by a projection vector $\mathbf{v} \in \mathbb{R}^D$:

$$y_i^l = \mathbf{v}^\top \mathbf{x}_i^l, \quad (2)$$

such that the correlation between N subjects (repetitions) is maximized. We define correlation as the ratio of the between-subject covariance, r_B , and the within-subject covariance, r_W :

$$\rho = \frac{1}{N-1} \frac{r_B}{r_W}. \quad (3)$$

The between-subject covariances are averaged over all pairs of subjects, and within-subject covariance is averaged over all subjects:

$$r_B = \sum_{l=1}^N \sum_{k=1, k \neq l}^N \sum_{i=1}^T (y_i^l - \bar{y}_*^l)(y_i^k - \bar{y}_*^k), \quad (4)$$

$$r_W = \sum_{l=1}^N \sum_{i=1}^T (y_i^l - \bar{y}_*^l)(y_i^l - \bar{y}_*^l), \quad (5)$$

where, $\bar{y}_*^l = \frac{1}{T} \sum_{i=1}^T y_i^l$, is the sample-mean for subject l . The factor $(N-1)^{-1}$ in definition (3) is required so that correlation is normalized to $\rho \leq 1$ (see Appendix C.2). To simplify the notation, in our “variance” and “covariance” definitions we will generally omit common scaling factors, in this case, $(T-1)^{-1}N^{-1}$.

We will refer to ρ as the inter-subject correlation (ISC), but it could also be termed the inter-rater correlation or inter-repeat correlation (IRC) depending on the context. In Appendix C.1 we discuss this definition of correlation and its relation to other measures of correlation, such as intra-class correlation or Pearson’s correlation coefficient. Note that r_W is also the variance around the subject-mean. By inserting Eq. (2) into definition (3) it follows readily that

$$\rho = \frac{1}{N-1} \frac{\mathbf{v}^\top \mathbf{R}_B \mathbf{v}}{\mathbf{v}^\top \mathbf{R}_W \mathbf{v}}, \quad (6)$$

where \mathbf{R}_B and \mathbf{R}_W are the between-subject and within-subject covariance matrices of \mathbf{x}_i^k defined analogously to (4)-(5):

$$\mathbf{R}_B = \sum_{i=1}^T \sum_{l=1}^N \sum_{k=1, k \neq l}^N (\mathbf{x}_i^l - \bar{\mathbf{x}}_*^l)(\mathbf{x}_i^k - \bar{\mathbf{x}}_*^k)^\top, \quad (7)$$

$$\mathbf{R}_W = \sum_{i=1}^T \sum_{l=1}^N (\mathbf{x}_i^l - \bar{\mathbf{x}}_*^l)(\mathbf{x}_i^l - \bar{\mathbf{x}}_*^l)^\top. \quad (8)$$

Here $\bar{\mathbf{x}}_*^l = \frac{1}{T} \sum_{i=1}^T \mathbf{x}_i^l$ is the sample-mean for subject l . The projection vector \mathbf{v} that maximizes ρ can be found as the solution of $\partial \rho / \partial \mathbf{v}^\top = 0$, which yields:

$$\mathbf{R}_B \mathbf{v} = \mathbf{R}_W \mathbf{v} \rho. \quad (9)$$

Given that \mathbf{R}_W is invertible, \mathbf{v} is an eigenvector of $\mathbf{R}_W^{-1}\mathbf{R}_B$ with eigenvalue ρ . Maximal inter-subject correlation is achieved by projecting the data onto the eigenvector of $\mathbf{R}_W^{-1}\mathbf{R}_B$ with maximal eigenvalue. Note that there are multiple eigenvectors, $\mathbf{v}_d, d = 1 \dots D$, that satisfy this equation. The full set of solutions to this equation is written as

$$\mathbf{R}_B \mathbf{V} = \mathbf{R}_W \mathbf{V} \mathbf{\Lambda}, \quad (10)$$

where the eigenvectors \mathbf{v}_d are the columns of matrix \mathbf{V} , and $\mathbf{\Lambda}$ is a diagonal matrix. The diagonal elements of this matrix are the inter-subject correlation, ρ_d , of the corresponding projections of the data, $y_d = \mathbf{v}_d^\top \mathbf{x}$. Note that these additional projections of the data are uncorrelated because their correlation matrix, \mathbf{R}_W^y — defined as in Eq. (8) but for \mathbf{y} — is diagonal:

$$\mathbf{R}_W^y = \mathbf{V}^\top \mathbf{R}_W \mathbf{V} = \mathbf{\Lambda}_W. \quad (11)$$

The fact that $\mathbf{\Lambda}_W$ is a diagonal matrix is a well-know property of the generalized eigenvalue equation (9) (see Appendix A.1).

To summarize, the principal eigenvector of the between-subject over the within-subject covariance matrices provides the projection of the data that maximizes inter-subject correlation. Subsequent smaller eigenvectors provide additional projections of the data that are uncorrelated with one another. The corresponding eigenvalues are equal to the inter-subject correlation that each projection achieves. It follows that the last projection captures the direction with the smallest inter-subject correlation. Note that the corresponding projections are uniquely defined, provided that the ISC are distinct (see Appendix A.3). In the illustrative example of Fig. 1 with $D = 2$, the eigenvalues were $\rho_1 = 1$ and $\rho_2 = 0.004$, respectively.

An application of CorrCA to the problem of identifying brain activity that is shared between subjects during watching of videos is described in Section 11.1.

4. Fast computation of inter-subject correlation

In Eq. (7), the term $k = l$ is excluded from the sum over k . Note that the excluded term is precisely \mathbf{R}_W , so that adding the two covariances together completes a sum with all pairs, including $k = l$. We will refer to this, therefore, as the total covariance:

$$\mathbf{R}_T = \mathbf{R}_B + \mathbf{R}_W \quad (12)$$

$$= \sum_{i=1}^T \sum_{l=1}^N \sum_{k=1}^N (\mathbf{x}_i^l - \bar{\mathbf{x}}_*^l)(\mathbf{x}_i^k - \bar{\mathbf{x}}_*^k)^\top. \quad (13)$$

This relationship is useful because \mathbf{R}_T can be simplified to:

$$\mathbf{R}_T = N^2 \sum_{i=1}^T (\bar{\mathbf{x}}_i^* - \bar{\mathbf{x}}_*^*)(\bar{\mathbf{x}}_i^* - \bar{\mathbf{x}}_*^*)^\top, \quad (14)$$

where $\bar{\mathbf{x}}_i^* = \frac{1}{N} \sum_{l=1}^N \mathbf{x}_i^l$ and $\bar{\mathbf{x}}_*^* = \frac{1}{T} \sum_{i=1}^T \bar{\mathbf{x}}_i^*$ are the mean across subjects and the grand mean, respectively. Thus, to compute inter-subject correlation, one actually never has to

consider pairs of subjects, because \mathbf{R}_B can be computed from \mathbf{R}_T and \mathbf{R}_W , and neither one requires a sum over pairs of subjects. This makes the computation more efficient than the direct implementation of Eqs. (7)-(8), which has been used in previous work (Dmochowski et al., 2012, 2014, 2015; Tanaka et al., 2013; Cohen and Parra, 2016).

5. Relationship to Linear Discriminant Analysis

Perhaps the naming and the additivity of the covariance matrices introduced here — Eqs. (7), (8), (12) — reminds some readers of the between-class and within-class scatter matrices used in Linear Discriminant Analysis (LDA). In the current notation these are:

$$\mathbf{S}_T = \sum_{i=1}^T \sum_{l=1}^N (\mathbf{x}_i^l - \bar{\mathbf{x}}_*) (\mathbf{x}_i^l - \bar{\mathbf{x}}_*)^\top \quad (15)$$

$$\mathbf{S}_B = \sum_{i=1}^T N (\bar{\mathbf{x}}_i^* - \bar{\mathbf{x}}_*) (\bar{\mathbf{x}}_i^* - \bar{\mathbf{x}}_*)^\top \quad (16)$$

$$\mathbf{S}_W = \sum_{i=1}^T \sum_{l=1}^N (\mathbf{x}_i^l - \bar{\mathbf{x}}_i^*) (\mathbf{x}_i^l - \bar{\mathbf{x}}_i^*)^\top. \quad (17)$$

Here, index i enumerates the different classes and index l enumerates the exemplars in each class (see Table 2 for an overview on the use indices in different algorithms). Therefore $\bar{\mathbf{x}}_i^* = \frac{1}{N} \sum_{l=1}^N \bar{\mathbf{x}}_i^l$, and, $\bar{\mathbf{x}}_*^* = \frac{1}{T} \sum_{i=1}^T \bar{\mathbf{x}}_i^*$, are the class mean and grand mean vectors, respectively. Scatter matrices also satisfy an additivity rule: $\mathbf{S}_T = \mathbf{S}_B + \mathbf{S}_W$ (Duda et al., 2012). The goal of LDA is to maximize the separation between classes, which is measured by

$$S = \frac{\mathbf{v}^\top \mathbf{S}_B \mathbf{v}}{\mathbf{v}^\top \mathbf{S}_W \mathbf{v}}. \quad (18)$$

As before, the maximal separation S is obtained for the eigenvector of $\mathbf{S}_B^{-1} \mathbf{S}_W$ with the maximum eigenvalue S . In the case of multiple classes, multiple eigenvectors provide a subspace that best separates the multiple classes. This concept was first proposed by Rao (1948) and generalizes the case of two classes introduced by Fisher (1936).

This optimality criterion and resulting eigenvalue problem look strikingly similar to that of CorrCA in (6). Despite the similar naming, however, the scatter matrices differ from the between-subject and within-subject covariance matrices, and it is not immediately obvious how the two optimality criteria relate to one another. There is, however, a close relationship between the two (see Appendix B):

$$N \mathbf{S}_B = \mathbf{R}_W + \mathbf{R}_B, \quad (19)$$

$$N \mathbf{S}_W = (N-1) \mathbf{R}_W - \mathbf{R}_B + N T \mathbf{S}_M, \quad (20)$$

where \mathbf{S}_M is the covariance of $\bar{\mathbf{x}}_*^l$ across subjects:

$$\mathbf{S}_M = \sum_{l=1}^N (\bar{\mathbf{x}}_*^l - \bar{\mathbf{x}}_*) (\bar{\mathbf{x}}_*^l - \bar{\mathbf{x}}_*)^\top. \quad (21)$$

When these mean values are equal across subjects, e.g. when they are zero-mean, then the scatter matrices are a linear combination of the between- and within-subject covariance matrices. Under this assumption, we can also write a simple functional relationship between class separation S and inter-subject correlation ρ :

$$S = \frac{r_W + r_B}{(N-1)r_W - r_B} = \frac{\rho + (N-1)^{-1}}{1 - \rho}. \quad (22)$$

Note that this relationship is monotonically increasing, for $\rho \leq 1$, because the slope of this relationship is strictly positive:

$$\frac{\partial S}{\partial \rho} = \frac{N}{N-1} \frac{1}{(1-\rho)^2}. \quad (23)$$

This means that maximizing class separation S in (18) also results in maximal inter-subject correlation ρ , provided we equalize the means. In fact, finding vectors \mathbf{v} that maximize S of Eq. (18) gives the same set of solutions as maximizing ρ of Eq. (6).

To see this, note that the goal of maximizing a ratio of two matrices, such as in Eq. (6), can also be achieved by joint-diagonalization of these two matrices (see Appendix A.1):

$$\begin{aligned} \mathbf{V}^\top \mathbf{R}_B \mathbf{V} &= \mathbf{\Lambda}_B, \\ \mathbf{V}^\top \mathbf{R}_W \mathbf{V} &= \mathbf{\Lambda}_W, \end{aligned} \quad (24)$$

where $\mathbf{\Lambda}_B$ and $\mathbf{\Lambda}_W$ are diagonal matrices. Note that if \mathbf{V} jointly diagonalizes two matrices, it also diagonalizes any linear combinations of the two (Fukunaga, 2013, see Appendix A.2). Because \mathbf{S}_B and \mathbf{S}_W are linear combination of \mathbf{R}_B and \mathbf{R}_W , then the \mathbf{V} that satisfies (24) also diagonalizes \mathbf{S}_B and \mathbf{S}_W . Thus, this \mathbf{V} captures the eigenvectors to $\mathbf{R}_W^{-1} \mathbf{R}_B$ as well as $\mathbf{S}_W^{-1} \mathbf{S}_B$, and because the eigenvalues of the two problems are monotonically related, the eigenvectors will be sorted in the same order for both problems. Thus, the solutions to both optimization problems are the same. To summarize, CorrCA and LDA yield the same result, provided that sample-means are equal across subjects, e.g. zero mean.

6. Correlated Component Analysis finds components with maximum reliability

In the present context, the scatter matrices \mathbf{S}_B and \mathbf{S}_W are interesting for another, perhaps more important reason. Consider the case where l represents repeated measurements of raters, or repeated measures on the same subjects, so that ρ now measures inter-rater correlation, or inter-repeat correlation (IRC). According to Eq. (16), \mathbf{S}_B measures (except for a scaling factor) the sample-covariance of $\bar{\mathbf{x}}_i^*$, which is the mean across repeats. On the other hand, according to Eq. (17), \mathbf{S}_W measures the sample-covariance averaged over repeats. When projected onto y with \mathbf{v} they define the variance of the mean across repeats, σ_y^2 , and average variance around these means, $\bar{\sigma}_y^2$, respectively. The ratio of the two variances is a sensible definition for signal-to-noise ratio (SNR):

$$S = \frac{\sigma_y^2}{\bar{\sigma}_y^2}. \quad (25)$$

CorrCA	LDA	JD
$\rho = \frac{1}{N-1} \frac{\mathbf{v}^\top \mathbf{R}_B \mathbf{v}}{\mathbf{v}^\top \mathbf{R}_W \mathbf{v}}$	$S = \frac{\mathbf{v}^\top \mathbf{S}_B \mathbf{v}}{\mathbf{v}^\top \mathbf{S}_W \mathbf{v}} \stackrel{*}{=} \frac{\rho + (N-1)^{-1}}{1-\rho}$	$\frac{\mathbf{v}^\top \mathbf{S}_B \mathbf{v}}{\mathbf{v}^\top \mathbf{S}_T \mathbf{v}} \stackrel{*}{=} (N-1)\rho + 1$

Table 1: Relationship between the optimality criteria of different algorithms. ρ is inter-subject correlation, and S is class-separation. * assuming zero-mean signals, or unbiased raters ($\mathbf{S}_M = 0$).

We take this SNR also as a metric of repeat-reliability. In this view, the results of the previous section show that maximizing correlation between repeats is equivalent to maximizing repeat-reliability. In particular, Eq. (23) provides the relationship between SNR and IRC.

An application of CorrCA to the problem of identifying ratings that are reliably reproduced between different raters is described in Sections 11.2 and 11.3. In Section 11.4 we describe results on the problem of identifying components of brain activity with maximal SNR.

A similar joint diagonalization approach was presented in (de Cheveigné and Parra, 2014) with the goal of maximizing signal-to-noise ratio. For a specific form of denoising (averaging over trials) the approach diagonalizes matrices \mathbf{S}_T and \mathbf{S}_B . By the same argument as above it is clear that it provides the same solution as LDA. The optimization criteria for the two techniques is summarized in Table 1 along with the Joint-Decorrelation (JD) approach of (de Cheveigné and Parra, 2014).

7. Extension to non-linear maps using Kernels

So far we have only considered linear transformations between \mathbf{x} and \mathbf{y} . Now, given the close relationship between CorrCA and LDA, we can extend CorrCA to non-linear transformations following the approach of kernel-LDA (Mika et al., 1999; Baudat and Anouar, 2000; Zhang et al., 2004). Assume a non-linear mapping $\Phi(\cdot)$ for the data of subject l :

$$\mathbf{Z}^l = \Phi(\mathbf{X}^l). \quad (26)$$

In this notation, \mathbf{X}^l has dimension $D \times T$ spanning the entire multivariate time series for subject l , and \mathbf{Z}^l has dimensions $D' \times T'$. Thus, the non-linear transformation $\Phi(\cdot)$ is a mapping from space-time to a new space with possibly quite different dimensions.¹ The approach now is to first extract non-linear features of the data with $\Phi(\cdot)$, and then combine these features linearly with projection \mathbf{v} :

$$\mathbf{y}^l = \mathbf{v}^\top \mathbf{Z}^l. \quad (27)$$

1. In the example of brain signals, \mathbf{Z}^l could represent, for instance, the power spectrum in source space (Michel et al., 2004), where D' captures the number of sources and T' the number of frequency bins. In the application examples and in the code we simplify this by applying the non-linear mapping to each time point separately, so that $T = T'$ and we have a purely spatial nonlinear mapping, similar to conventional kernel-LDA. However, this more general formulation allows one in principle to reduce the time dimension as well. This is important because the computational complexity of the kernel approach scales with $O(T^3)$, and thus becomes prohibitive for long time-domain signals.

Note that the transformation $\Phi(\cdot)$ does not need to be defined explicitly. Instead, the “kernel trick” (Schölkopf et al., 1998) allows one to specify this non-linearity only implicitly, by defining instead the inner product of vectors in this new D' -dimensional feature space with a kernel function $\mathbf{K}(\cdot, \cdot)$:

$$\mathbf{Z}^k{}^\top \mathbf{Z}^l = \mathbf{K}(\mathbf{X}^k, \mathbf{X}^l). \quad (28)$$

Knowing how to compute the inner product is sufficient, if all the expressions in the algorithm can be formulated in terms of this inner product.² In a slight abuse of notation, we will write $\mathbf{K}^{kl} = \mathbf{K}(\mathbf{X}^k, \mathbf{X}^l)$ as shorthand for this matrix defined for each pair of subjects lk . Note that the dimensions of \mathbf{K}^{kl} are $T' \times T'$ and thus this matrix can potentially be quite large. In cases where the non-linear transformation $\Phi(\cdot)$ can be expressed explicitly, and $D' \ll T'$, one may chose to operate directly with \mathbf{Z}^l . Otherwise, it will be beneficial to leverage the definition of the non-linear transformation in terms of \mathbf{K}^{kl} . In the following, we will rewrite the optimization criterion ρ in terms of \mathbf{K}^{kl} alone.

The crucial step is to define the projection vectors in terms of the samples of the mean across subjects.

$$\mathbf{v} = \sum_{i=1}^{T'} \alpha_i \bar{\mathbf{z}}_i^* = \bar{\mathbf{Z}}^* \boldsymbol{\alpha}, \quad (29)$$

where $\bar{\mathbf{z}}_i^*$ is the across-subject mean vector for exemplar i in the non-linear mapped space (i th column of $\bar{\mathbf{Z}}^*$). Here, α_i are parameters that indicate how exemplars $\bar{\mathbf{z}}_i$ are to be combined to represent the projection vector \mathbf{v} . The approach will be to find optimal vector $\boldsymbol{\alpha}$ instead of vector \mathbf{v} , and thus we need to rewrite the optimality criterion in term of $\boldsymbol{\alpha}$.³ Combining (27) with (29) one can now express the non-linear components \mathbf{y} as a linear combination of \mathbf{K}^{lk} as follows:

$$\begin{aligned} \mathbf{y}^l &= \mathbf{v}^\top \mathbf{Z}^l = \boldsymbol{\alpha}^\top \frac{1}{N} \sum_{k=1}^N \mathbf{Z}^k{}^\top \mathbf{Z}^l \\ &= \boldsymbol{\alpha}^\top \frac{1}{N} \sum_{k=1}^N \mathbf{K}^{kl} = \boldsymbol{\alpha}^\top \bar{\mathbf{K}}^{*l}, \end{aligned} \quad (31)$$

2. Note that this inner product is only over dimension D' . The function $\mathbf{K}(\cdot, \cdot)$ is therefore only a “kernel” in this D' dimensional space.

3. As an alternative to (29), we could have also defined the projection vector in terms of the samples of all subjects:

$$\mathbf{v} = \sum_{l=1}^N \sum_{i=1}^{T'} \alpha_i^l \mathbf{z}_i^l. \quad (30)$$

The derivations can all be repeated analogously and the resulting algorithm is the same, but with NT' degrees for freedom in $\boldsymbol{\alpha}$. In the provided code, this is referred to as the “full model”, whereas equations derived here for the expansion in terms of the mean (29) are referred to as the “mean model”. In the example provided in Figure 2, the numerical results are very similar for both models. The question as to whether the mean model is sufficient is empirical and comes down to whether there is enough diversity in the mean response to capture the individual variations across subjects. Mathematically, this implies that the expansion in terms of the mean is complete, i.e., the mean response matrix $\bar{\mathbf{Z}}^*$ is full rank.

where the bar in $\bar{\mathbf{K}}^{*l}$, indicates that we are taking the mean, and the asterisk specifies over which index this mean is taken. It analogously follows that,

$$\mathbf{v}^\top \bar{\mathbf{Z}}^* = \boldsymbol{\alpha}^\top \bar{\mathbf{K}}^{**}. \quad (32)$$

Denote the columns of matrix \mathbf{Z}^l and $\bar{\mathbf{K}}^{*l}$ as \mathbf{z}_i^l and $\bar{\mathbf{k}}_i^{*l}$. Then we can also write with this notation for the average:

$$\mathbf{v}^\top \bar{\mathbf{z}}_i^* = \boldsymbol{\alpha}^\top \bar{\mathbf{k}}_i^{**}. \quad (33)$$

The within-subject and total variance of the non-linear features \mathbf{z}_i^l can thus be written as:

$$\begin{aligned} r_W &= \mathbf{v}^\top \mathbf{R}_W \mathbf{v} = \sum_{l=1}^N \sum_{i=1}^{T'} \mathbf{v}^\top (\mathbf{z}_i^l - \bar{\mathbf{z}}_*^l) (\mathbf{z}_i^l - \bar{\mathbf{z}}_*^l)^\top \mathbf{v} \\ &= \boldsymbol{\alpha}^\top \mathbf{C}_W \boldsymbol{\alpha}, \end{aligned} \quad (34)$$

$$\begin{aligned} r_T &= \mathbf{v}^\top \mathbf{R}_T \mathbf{v} = N^2 \sum_{i=1}^{T'} \mathbf{v}^\top (\bar{\mathbf{z}}_i^* - \bar{\mathbf{z}}_*^*) (\bar{\mathbf{z}}_i^* - \bar{\mathbf{z}}_*^*)^\top \mathbf{v} \\ &= \boldsymbol{\alpha}^\top \mathbf{C}_T \boldsymbol{\alpha}, \end{aligned} \quad (35)$$

where we defined the within-subject and total covariance of \mathbf{k}_i^{*l} as:

$$\mathbf{C}_W = \sum_{l=1}^N \sum_{i=1}^{T'} (\bar{\mathbf{k}}_i^{*l} - \bar{\mathbf{k}}_*^{*l}) (\bar{\mathbf{k}}_i^{*l} - \bar{\mathbf{k}}_*^{*l})^\top, \quad (36)$$

$$\mathbf{C}_T = N^2 \sum_{i=1}^{T'} (\bar{\mathbf{k}}_i^{**} - \bar{\mathbf{k}}_*^{**}) (\bar{\mathbf{k}}_i^{**} - \bar{\mathbf{k}}_*^{**})^\top. \quad (37)$$

Because of the symmetry of these expressions with the definitions of \mathbf{R}_W and \mathbf{R}_T , we have again, $\mathbf{C}_B = \mathbf{C}_T - \mathbf{C}_W$, and can therefore write the inter-subject correlation in the non-linear space as a function of the new parameters $\boldsymbol{\alpha}$ as follows:

$$\rho = \frac{\mathbf{v}^\top \mathbf{R}_B \mathbf{v}}{\mathbf{v}^\top \mathbf{R}_W \mathbf{v}} = \frac{\boldsymbol{\alpha}^\top \mathbf{C}_B \boldsymbol{\alpha}}{\boldsymbol{\alpha}^\top \mathbf{C}_W \boldsymbol{\alpha}}. \quad (38)$$

This can be solved again as an eigenvalue problem but now with the within- and between-subject covariance matrices of the kernel vectors $\bar{\mathbf{k}}_i^{*l}$ and the corresponding projection vector $\boldsymbol{\alpha}$.

To demonstrate the method, we generated a simple 2-dimensional example where the shared dimension is non-linear. As with the example for linear CorrCA (Figure 1), we have simulated $N = 2$ “subjects”, each providing two signals ($D = 2$), now with $T = 40$ samples in time (Figure 2 A & B). In this case the two subjects share the amplitude (distance from the origin in the 2-dimensional input space of \mathbf{x} ; see Figure 2 C). However, the phase angle in this 2-dimensional plane is selected randomly at each time point and for each subject. We apply kernel-CorrCA keeping the time axis unchanged ($T = T'$).¹ The first component dimension, y_1 , is approximately linear with the amplitude and is independent of phase in the original 2D plane (Figure 2 G & H). This component therefore perfectly captured

the amplitude as the shared non-linear dimension. The second component dimension, y_2 is essentially a nonlinear function of component y_1 (Figure 2 F), hence it also has high ISC. The specific non-linearity is arbitrary, but does enforce that the two variables are uncorrelated. We obtain nearly identical results regardless of whether we use Gaussian or Tanh kernels (see code and Zhang et al., 2004), although the specific relationship between y_1 and y_2 differs.

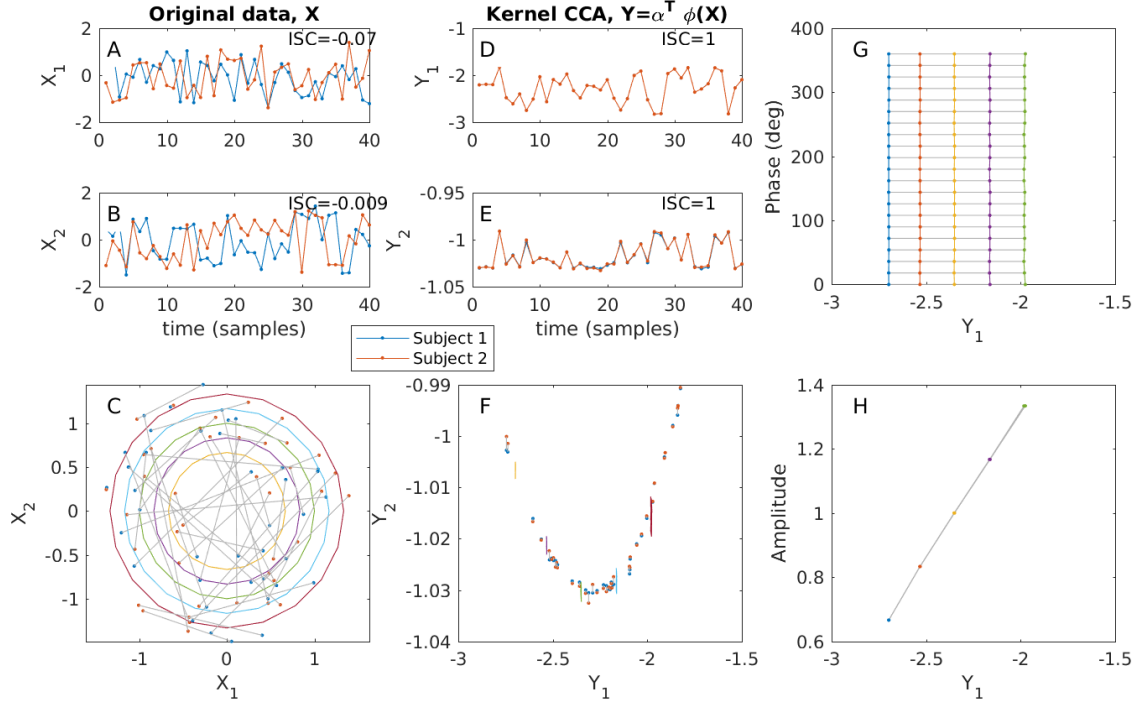


Figure 2: Kernel CorrCA. In this demonstrative 2D example, two subjects share amplitude but have a random phase. The goal is to extract that common amplitude signal — a non-linear transformation of the data — from 60 samples. (A-B) Two dimensions of the original data with one trace for each subject. (C) Samples are connected between the two subjects with gray lines, as in Figure 1. Circles of varying radii are drawn for visualization purposes. Note that connected points have the same distance from the centers, i.e. subjects share an amplitude. (D-E) After kernel CorrCA, signals between subjects are strongly correlated (ISC=1). (F) Points are in a new non-linear space, which is necessarily curved to decorrelate the two dimensions. (G-H) Colored lines correspond to the circles in panel C. The first dimension y_1 is independent of phase and grows linearly with amplitude. This means that the algorithm identified the non-linear dimension that is shared between the two subjects.

8. Regularization and robustness

A common numerical difficulty with generalized eigenvalue problems is the required matrix inverse. In the case of CorrCA, it is necessary to invert \mathbf{R}_W in equation (9). When some of the eigenvalues are small (or even zero), then random fluctuations due to noise will dominate in the inverse. It is thus important to regularize the estimate of \mathbf{R}_W . In the past, we have used the Truncated Singular Value Decomposition (TSVD) (Hansen, 1994) and shrinkage (Ledoit and Wolf, 2004) for this purpose (Dmochowski et al., 2012, 2014; Ki et al., 2016; Cohen and Parra, 2016).

Note that a high inter-subject correlation corresponds to large eigenvalues of $\mathbf{R}_W^{-1}\mathbf{R}_B$. These eigenvalues will be large if the selected direction exhibits large power in the space of \mathbf{R}_B , or *low* power in the space of \mathbf{R}_W . The former is meaningful and desired, but the latter can occur with rank-deficient or impoverished data and may lead to spuriously high inter-subject correlation. Truncating the eigenvalue spectrum of \mathbf{R}_W has the desired effect of forcing the extracted data dimensions to have both high power in \mathbf{R}_B and \mathbf{R}_W . This makes it less likely to find spuriously reliable dimensions. Formally, the TSVD approach is to select \mathbf{V} according to:

$$\mathbf{R}_B\mathbf{V} = \tilde{\mathbf{R}}_W\mathbf{V}\mathbf{\Lambda}, \quad (39)$$

where the within-subject covariance is now regularized with the following approximation:

$$\tilde{\mathbf{R}}_W = \tilde{\mathbf{U}}_W\tilde{\mathbf{\Lambda}}_W\tilde{\mathbf{U}}_W^\top, \quad (40)$$

where $\tilde{\mathbf{U}}_W = [\mathbf{u}_1 \dots \mathbf{u}_K]$, and $\tilde{\mathbf{\Lambda}}_W = \text{diag}[\lambda_1 \dots \lambda_K]$ are the K principal eigenvectors of \mathbf{R}_W and associated eigenvalues. The inverse of \mathbf{R}_W is computed according to:

$$\tilde{\mathbf{R}}_W^{-1} = \tilde{\mathbf{U}}_W\tilde{\mathbf{\Lambda}}_W^{-1}\tilde{\mathbf{U}}_W^\top, \quad (41)$$

which then left-multiplies (39) and yields the regularized solution to the CorrCA problem.

The parameter K is the number of eigenvectors to retain in the representation of \mathbf{R}_W . Decreasing this number strengthens the level of regularization, and $K = D$ is equivalent to not regularizing.

Shrinkage regularization operates by a similar principle: dimensions of the data exhibiting low variance (corresponding to low eigenvalues of \mathbf{R}_W) are enriched by incrementing these eigenvalues:

$$\tilde{\mathbf{R}}_W = \mathbf{U}_W\tilde{\mathbf{\Lambda}}_W\mathbf{U}_W^\top, \quad (42)$$

where $\tilde{\mathbf{\Lambda}}_W = (1 - \gamma)\mathbf{\Lambda}_W + \gamma\bar{\lambda}\mathbf{I}$, γ is the shrinkage parameter with $0 \leq \gamma \leq 1$, and $\bar{\lambda} = \text{Tr}(\mathbf{R}_W)/D$ is the mean eigenvalue of the (unregularized) within-subjects covariance. The effect of shrinkage, which retains the full dimensionality of the covariance matrix, is that the smaller eigenvalues are increased and larger eigenvalues are reduced (hence the term “shrinkage”).

The advantage of shrinkage regularization is the simplicity of its implementation, where the regularized covariance can be simply computed as

$$\tilde{\mathbf{R}}_W = (1 - \gamma)\mathbf{R}_W + \gamma\bar{\lambda}\mathbf{I} \quad (43)$$

without any further modifications to the generalized eigenvalue routine. TSVD instead requires more careful handling of the null-space when computing the general eigenvalues (see provided code). On the other hand, TSVD has the important advantage that the solutions \mathbf{V} to the regularized eigenvalue problem (39) diagonalize $\tilde{\mathbf{R}}_W$ as well as the original \mathbf{R}_W . This means that the extracted components are strictly uncorrelated, whereas for shrinkage that is only approximately the case.

The performance of TSVD and shrinkage can be evaluated by maximizing ISC on one data set (training set) and using the resulting projection vectors to measure ISC on a different data set (test set). We do this on one of the application examples in Section 11.5.

9. Testing for statistical significance

Given a set of extracted correlated components, the question arises as to how many of these components exhibit statistically significant correlations. The assessment of statistical significance of ρ requires knowledge of their distribution under the null hypothesis. The null hypothesis associated with CorrCA states that there exists no shared one-dimensional subspace in which the data of at least two subjects are correlated. Estimating the null distribution is complicated by two factors. First, CorrCA has free parameters, the optimization of which inflates the ISC values under the null hypothesis to an extent governed by the dimensionality of the problem (parameters T , D , and N). Second, temporal correlations in the data lead to larger variances than expected under the assumption of independent and identically distributed (IID) data typical for parametric statistical tests, and, thereby, to false positive detections of significant ISC values. The IID assumption may be reasonable for rating data, where rated individuals may be independent from one another, but it is not fulfilled for time series data such as EEG recordings. Here, we present three approaches to estimate the significance of individual correlated components as well as the dimensionality of the correlated subspace for IID as well as auto-correlated data.

Phase-scrambled surrogate data—This approach was introduced by Theiler et al. (1992) as a tool to test for nonlinearities in time series data. The idea is to create data that are consistent with the null hypothesis but otherwise resemble the observed experimental data in terms of temporal and spatial correlations. The original surrogate data of Theiler et al. (1992) preserves the amplitude spectrum of the original data but uses a random phase spectrum, which is achieved through an application of the Fourier transform and its inverse. This approach was extended to additionally maintain the spatial covariance structure of multivariate data by using identical random phase shifts for all variables by Prichard and Theiler (1994). Here, we use the approach of Prichard and Theiler to test for significant ρ based on the consideration that no inter-subject correlation can be present after phase-scrambling the data of each subject. Variants of this approach have previously been used to test for significant correlations (Schaworonkow et al., 2015; Ki et al., 2016; Cohen and Parra, 2016; Haufe et al., 2017). The p-value for the ISC of a given correlated component is defined as the frequency with which the ISC computed from the random-phase surrogate data is exceeded by the ISC of the most strongly correlated component in the original data.

Random circular shifts—A simpler approach to create surrogate data for CorrCA is to circularly shift the samples of each subject by a different offset, where the same offset is used

for all variables of the same subject. Just as the phase-scrambling approach, this procedure ensures that spatial correlations and spectral properties of the original data are maintained. Additionally, non-linear properties of the original data are maintained. This approach has previously been used in Dmochowski et al. (2012, 2014). P-values are defined analogous to the phase-scrambling approach.

Parametric null distribution—For IID data, a parametric statistical test can be devised. Here, we use the fact that S is a ratio of variances, as emphasized in Eq. (25). After appropriate scaling it corresponds to a F -statistic, as used in the analysis of variance (ANOVA) (Fisher, 1925):

$$F = \frac{T(N-1)}{T-1}S, \quad (44)$$

with degrees of freedom $d_1 = T(N-1)$ and $d_2 = T-1$ (Papoulis and Pillai, 2002). This means that we can use the F -distribution to compute statistical significance for S (or from ρ , using Eq. (23), provided the means are equalized, i.e. $\bar{\mathbf{x}}_*^l = \bar{\mathbf{x}}_*^*$). Evidently, this result does not hold for training data that has been leveraged to optimize this statistic itself. However, we can use the optimal projection vectors to assess statistical significance on separate, previously unseen test data. An important limitation is that the T exemplars have to be independent. This is true perhaps for rating data, but typically not true for temporal signals, where samples in time are often correlated. For such data, the non-parametric test discussed above are more appropriate. To avoid overestimating the number of components due to multiple testing (there are always D components to be tested), we adopt a Bonferroni correction. This limits the family-wise error rate, i.e. the probability of making one or more false discoveries among the D tests. Thus, only S values with $p < \alpha/D$ are considered significant, where α is the desired significance level.

We will test the validity of the three methods on simulated data in Section 12. The goal is to determine under which conditions these methods determine the correct number of underlying correlated components.

10. Parameter interpretation

An important aspect of dealing with multivariate models is parameter interpretation. CorrCA is an example of a “backward model” in the sense that the input data are transformed by the model to yield an approximation of the signals of interest, in this case the correlated components. It shares this property with a host of other methods including PCA, ICA, LDA, etc. An alternative modeling strategy is “forward modeling”, variants of which are known as Factor Analysis or General Linear Modeling. Here, known variables of presumable influence are transformed by the model to yield a low-dimensional approximation of the measured multivariate data. Such models are typically more consistent with the physical process of data generation. In imaging, a “forward model” refers to the mapping from the source of an image to the actual measurement. For example, in complex imaging modalities such as computer tomography and magnetic resonance imaging, the forward model is given by the Radon and Fourier transforms, respectively. In the case of electromagnetic brain signals, a forward model often refers to the “image” that a current source in the brain makes on the sensors.

In the linear case, forward and backward models are both parameterized by one model weight per input dimension and components. For CorrCA, the backward model is summarized in the matrix \mathbf{V} for all components. A corresponding forward model can be defined as the projection \mathbf{A} that best recovers measurements \mathbf{x} from the components \mathbf{y} (Parra et al., 2002, 2005):

$$\hat{\mathbf{x}} = \mathbf{A}\mathbf{y}. \quad (45)$$

The least-squares estimate of this projection is

$$\hat{\mathbf{A}} = \mathbf{R}_W \mathbf{V} (\mathbf{V}^\top \mathbf{R}_W \mathbf{V})^{-1}. \quad (46)$$

The columns \mathbf{a}_k of this matrix capture how correlated a putative source \mathbf{y}_k is with the observed sensor recordings \mathbf{x} . This approach of recovering the forward model from the backward model is explained in more detail in Haufe et al. (2014), along with a discussion on how forward and backward model parameters need to be interpreted.

The utility of the forward model is demonstrated for the case of brain activity, where we ask how the brain activity of a specific component manifests at the sensor level (Section 11.1). The utility of the backward model is demonstrated for the case of ratings, where we ask which rating items contribute the most to a reliable aggregate scores (Sections 11.2 and 11.3). It should be noted that when the original data is uncorrelated, such as in the rating data of Figure 5, then \mathbf{R}_W is already diagonal (see panel D). In that case then forward and backward models are identical, except of an overall scale for each component.

11. Applications

11.1 Extract brain activity that correlates between subjects

We have previously used CorrCA to analyze brain signals recorded from multiple subjects using electroencephalography (Dmochowski et al., 2012, 2014; Ki et al., 2016; Cohen and Parra, 2016; Poulsen et al., 2017; Cohen et al., 2017b; Petroni et al., 2018; Iotzov et al., 2017). In these experiments, subjects watched movies or listened to narrated stories while brain activity was recorded with multiple sensors (electroencephalography (EEG) — electrical potentials measured at multiple locations on the scalp surface). CorrCA was then used to extract components that were most reliable across subjects. These experiments showed that brain signals are significantly correlated between subjects on a rapid time-scale of less than a second (signals were high-pass filtered at 0.5 Hz). While the inter-subject correlation (ISC) values are small ($\rho \approx 0.05$), these values are highly significant and very reliable across sessions (Dmochowski et al., 2012) even in realistic environments (Poulsen et al., 2017). Interestingly, the level of correlation between subjects as measured by ISC is indicative of how attentive subjects are towards the stimulus (Ki et al., 2016) and, therefore, predictive of how well individuals remember the content of the videos (Cohen and Parra, 2016, see Section C.3 for a definition of ISC for individual subjects). This ISC also predicts the retention of TV and online audiences (Dmochowski et al., 2014; Cohen et al., 2017b). This work will be reviewed in more detail in an upcoming publication (Cohen et al., 2017a). Here, we show the spatial distributions of the forward model for the first three components. (Figure 3). Color is indicative of how strongly the component activity correlates with the signals recorded on different electrodes across the scalp. These first three components reach

statistical significance at the $\alpha = 0.05$ level, measured using a non-parametric statistical test based on randomly shifted surrogate data (see Section 9). In this example, the CorrCA algorithm used data from $D = 64$ electrodes, $T = 50344$ time points and $N = 18$ subjects. These distributions are largely preserved across different movie stimuli (component 1 in Figure 3 is preserved in Figure 7 on a different stimulus and despite the noisier recordings). Component 1 and 2 are indicative of visual and auditory processing (Cohen and Parra, 2016; Ki et al., 2016).

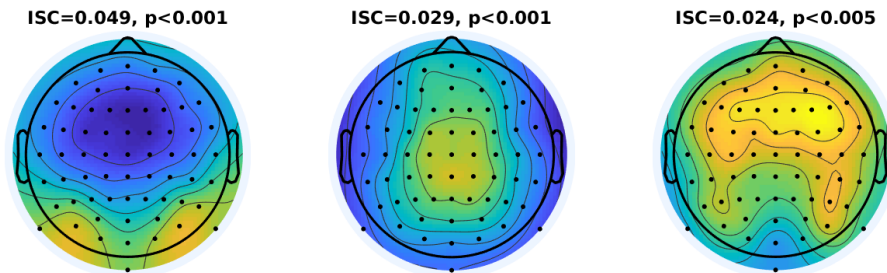


Figure 3: **Spatial distributions of correlated components of the EEG during video watching.** Correlated components maximize the inter-subject correlation of EEG responses to video clips (“Sunday at Rocco’s”, 2007, Storycorp). The video clip was approximately 197 seconds. This figure shows the “forward model” (see Section 10) corresponding to the three components with the strongest inter-subject correlation. Black points indicate locations of EEG electrodes. For details on these data see (Cohen and Parra, 2016). P-values were computed non-parametrically using randomly shifted surrogate data.

11.2 Maximize inter-rater reliability

The theory laid out in Section 6 shows that one can use CorrCA to identify components with maximal inter-rater reliability. In this following example, clinicians assessed the motor skill of children by measuring performance for various standard tasks (Zurich Neuromotor Assessment). The rating obtained for each task here is the time it takes the child to perform each task. This time is normalized relative to the values of a standard group of children of the same age (Rousson et al., 2008). Although this is an objective measure, there is nonetheless variability due to variable performance of the child when repeating the task, and also a subjective variability in the observer operating the stop-watch. In this specific data set, we have ratings from $T = 30$ children on $D = 12$ tasks from $N = 2$ raters. The 12 measures are mostly positively correlated across the children (Figure 4 A, see panel G for descriptive task labels). Reliability between raters is measured here as the inter-rater correlation (IRC), which differs across tasks (Figure 4 B).

The goal of CorrCA now is to find a (linear) combination of these 12 task ratings that provide a reliable overall aggregate score (one that is similar for the two independent raters). The resulting projection vectors \mathbf{V} are shown in Figure 4 G. Each column corresponds to a different component and has been normalized to have unit norm. Components are

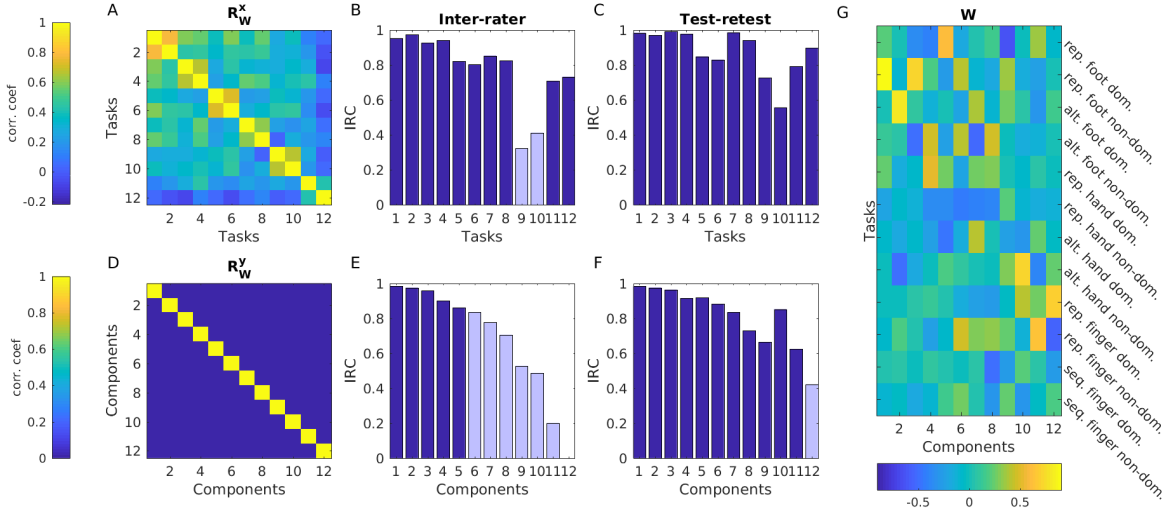


Figure 4: **Ratings from the Zurich Neuromotor Assessment** for $T = 30$ children, $D = 12$ tasks that were rated, and $N = 2$ clinical raters. The ratings are continuous numbers and normed by age. The goal of CorrCA is to identify aggregate scores that have high inter-rater correlation (IRC) and test-retest correlation. This is equivalent to maximizing inter-rater reliability and test-retest reliability. (A, B, C) Original rating data. (D, E, F) Component extracted with CorrCA. Dark-shaded bars indicated significant IRC (in panel E using circular shuffle statistics for training data; in panels B, C, F using F-statistics with Bonferroni correction; see Section 9) Data were provided by Valentin Rousson (Rousson et al., 2008). See text for details on each panel.

sorted in decreasing order of IRC (Figure 4 E) and therefore decreasing order of inter-rater reliability (see Section 6, Eq. 25). Of these components, the first five reach statistical significance at an α -level of 0.05 (highlighted in Figure 4 E). Inspecting the "backward model" \mathbf{V} it is clear that first component relies heavily on a single task (task 2, which has the highest IRC) but has small positive and negative contributions from other tasks. Components 2 and 3 are mostly a contrast between task 3 and 8, and 2 and 4, respectively. The detailed results can be obtained by running the code accompanying this article. In total, the method extracts different aggregate scores of high reliability, relying in some instances on a small subset of tasks. This has the potential of simplifying the assessment of motor performance while increasing its reliability. An important aspect of these various components is that, by design, they are uncorrelated to one another (uncorrelated across the 30 children; Figure 4 D), whereas the original task ratings all measures similar aspects (they are predominantly positively correlated; Figure 4 A).

In this data set, children were also evaluated a second time by the same rater in order to assess test-retest reliability (Figure 4 C). Comparing panels B and C, it is evident that the test-retest variability is somewhat higher than the inter-rater variability (i.e., the evaluation does indeed depend to some degree on the subjective judgment of the rater). The components extracted with the highest IRC also exhibit the strongest test-retest correlations (at

least for the first few components). This confirms that these aggregate measures generalize to data that was not used in the CorrCA optimization, and that minimizing subjective variability of the observer also minimizes test-retest variability.

11.3 Identify agreement between child and parent

We would like to provide an additional example of CorrCA on rating data. In this example, the goal is to identify questions on which parent and child agree. Specifically, we analyzed data collected with the Alabama Parenting Questionnaire (APQ) as part of the Healthy Brain Network initiative (Alexander et al., 2017). In the APQ, parents and children answered $D = 42$ questions pertaining to their relationship by providing a numerical value from 1 to 5 for each question. From this, the APQ averages various questions to provide aggregate scores related to different aspects: “involvement score”, “positive parenting score”, “poor supervision score”, “inconsistent discipline score”, and “corporal punishment score”. At time of this analysis, complete data were available for $T = 616$ children/parent pairs (ages 6-17, 40% female), i.e. $N = 2$ raters. The first observation on these data is that the answers from children and parents are only weakly correlated ($\rho = 0.17 \pm 0.1$, Figure 5 A). The aggregate scores fare even worse ($\rho = 0.064 \pm 0.13$). A two-sample t-test suggests that these aggregate scores are less reliably than individual questions ($t(47) = 2.4, p = 0.022$) including several scores with negative correlations. Evidently, children do not much agree with their parents when it comes to parenting issues, despite answering identical questions on the topic.

We applied CorrCA to find a combination of answers for which parents and children actually agree. To this end, we divided families at random into a training and a test set of equal size ($T = 308$) and computed the projections \mathbf{V} that maximized IRC on the training set. We then evaluated the resulting projections in terms of the correlation between child and parent for both train and test set (Figure 5 B & C). By design, IRC in the training set are large for the first components. On the test set, the first component also has a relatively large IRC, whereas the other components do not differ substantially in IRC from the original set of questions (IRC hovers around 0.2 in the original ratings, \mathbf{X} , and the aggregate component scores, \mathbf{Y}). The lower IRC values in the test set as compared to the training set indicate the presence of overfitting, although the discrepancy has been reduced here using shrinkage regularization (using $\gamma = 0.5$; see Section 8). To determine how many significantly correlated dimensions are actually present in these data, we used circular shuffle statistics (see Section 9) on all the data ($T = 616$) and found $K = 8$ components with $p < 0.05$. On the test data alone the F-statistics also found $K = 8$ significant components.

The component with the highest IRC ($\rho = 0.61$ on test set) has a combinations of questions contributing to reasonably reliable aggregate scores ($\rho = 0.61$, Figure 5 G). The following are four questions that contribute most strongly to this aggregate score of component 1 (weightings of \mathbf{V} in parenthesis): Question 32: “You are at home without an adult being with you” (-0.40); Question 21: “Your go out after dark without an adult with you” (-0.37); Question 11: “Your parent helps with your homework” (+0.37); Question 6: “You fail to leave a note or let your parents know where you are going” (-0.33). Positive weights indicate that the answers should have large scores to increase the value on this aggregate measure (and small scores for negative weights). Therefore, this measure seems to capture

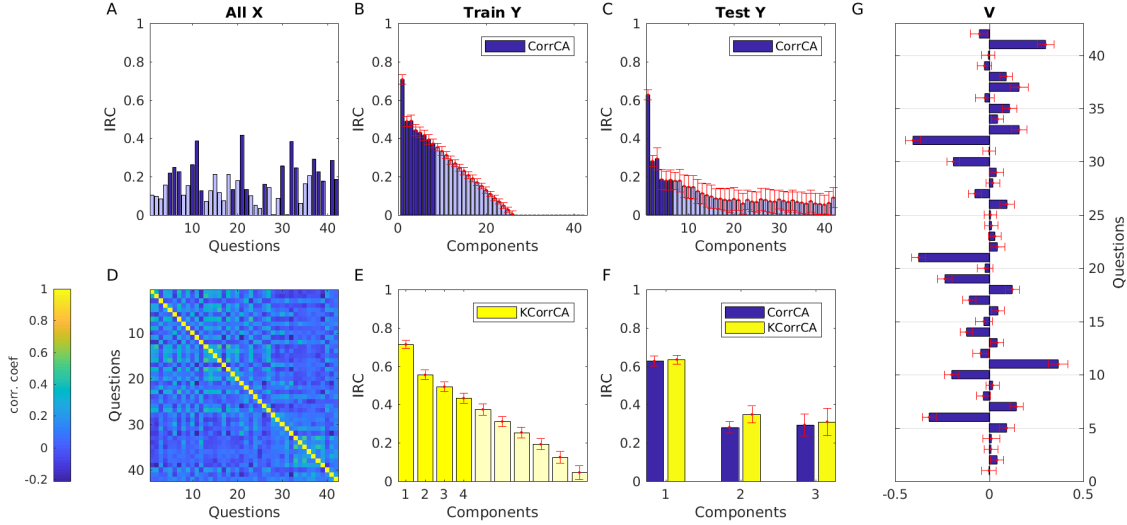


Figure 5: **Ratings from the Alabama Parenting Questionnaire** for $T = 616$ families and $D = 42$ questions, with $N = 2$ ratings from a child and one of its parents. Questions are answered on an integer scale from 1 to 5. Here, the goal of CorrCA is to maximize IRC, i.e., to identify agreement between children and parents. Data were collected by the Healthy Brain Networks Initiative (Alexander et al., 2017). Data were divided evenly and at random into a training and a test set. Second and third columns show results for training and test sets, respectively. Red error bars indicate the standard deviation across 100 random partitions of the data into training and test sets, and sampling with replacement within that (bootstrap estimates). Dark-shaded bars indicate significant IRC at $\alpha < 0.05$ (F-statistic, Bonferroni corrected with $T = 308$ for panels A and C; and circular shuffle statistic with $T = 616$ for panels B and E). (A) IRC between parent and child on all original questions. (B) IRC for the components extracted with CorrCA on the training set. Dark-shaded bars indicate significant IRC (circular shuffle statistic, $\alpha < 0.05$, $T = 616$). (C) IRC on the test set. Only the first component achieves strong IRC. In this case, we used shrinkage regularization ($\gamma = 0.5$, see Section 8). Dark-shaded bars indicate significant IRC (F-statistic, Bonferroni corrected, $\alpha < 0.05$, $T = 308$) (D) Correlation between questions across all 616 families. (E) Components extracted with kernel-CorrCA (Section 7). (F) Comparison of IRC on the test set for the 3 strongest components extracted with CorrCA and kernel-CorrCA. (G) Component weights for the strongest component extracted with CorrCA.

parent involvement versus independence of the child. In total, while parents and children largely disagreed, there is moderate agreement on how independent their lives are. Given this result, we suspected that this metric increases with the child’s age. Indeed, there is a strong correlation of this component with the child’s age across the cohort (Pearson’s

$r = 0.7$ and $r = 0.67$ for parent and child scores respectively, $p < 10^{-80}$, $T = 609$; with no significant difference with the child’s sex).

It should be noted that in this example one may have also used canonical correlation analysis, which provides a different projection vector to parent and child as they apparently differ in their judgment and thus may require different weighting of questions to find agreement.

We have also tested the non-linear kernel-CorrCA method on these data (Figure 5 E) as well as for the data presented in the next Section (11.4). In both instances, there was a small gain in terms of inter-rater correlation or inter-trial correlation respectively in the test data (Figure 5 F). However, the resulting component projection of the strongest components were not substantially different from the linear projections, suggesting that for these two examples there were no strong non-linear relationships in the data, at least for the kernels tested here.

11.4 Identify stimulus-related components in EEG with high SNR

PCA is often used to extract a low-dimensional representation of high-dimensional data. To this end, linear projections are sought so as to maximize the variance of the projected samples. When multiple repetitions of the data are collected, CorrCA can be used for the same purpose of reducing dimensionality of the data, but with the objective of capturing dimensions that are reliably reproduced across repetitions. Here we apply this to a conventional scenario in neuroimaging: neural activity is collected over time with multiple sensors, while the same experimental stimulus is repeated multiple times. We propose to use CorrCA to identify spatio-temporal patterns of activity that are well preserved across stimulus presentations (trials), similar to what was proposed in (Tanaka et al., 2013; de Cheveigné and Parra, 2014; Dmochowski et al., 2015; Dmochowski and Norcia, 2015). Ideally, the corresponding time-courses of multiple components are uncorrelated in time so that they capture different activity. CorrCA guarantees this by design as it diagonalizes \mathbf{R}_W . CorrCA is therefore similar to other source separation methods such as Independent Component Analysis (Makeig et al., 1996), Denoising Source Separation (Särelä and Valpola, 2005), or Joint-Decorrelation (de Cheveigné and Parra, 2014). In fact, CorrCA can be viewed as a form blind-source separation in that no labels are required for the analysis.

Here we analyze EEG data that were collected during an “Eriksen Flanker Task”. Subjects were presented with a collection of arrows pointing left or right. They were asked to decide as quickly as possible between two alternative choices (the direction of the center arrow) by pushing corresponding buttons with either their left or right hand. We analyze data of a single participant, who responded correctly in 550 trials, and made an error in 46 trials (Figure 6). This error, which participants notice as soon as they make their incorrect response, leads to a negative EEG potential 0-100ms after the button press (this period is indicated between black and red vertical lines in Figure 6 B & C for electrode #7, see electrode location in panel H). This phenomenon is known as the “error-related negativity” (ERN, Yeung et al., 2004). Button pushes also elicit the “readiness potential” — a gradually increasing voltage fluctuation preceding the button push at $t = 0ms$. Aside of the readiness potential and error-related negativity there are a series of other potential deflections following the button push. In this example, we have $T = 176$ time samples, $D = 64$ electrodes,

and $N = 46$ trials. Time is aligned across trials so that a specific event always occurs at the same time (in this case, a button press at time $t = 0ms$). The traditional approach to analyzing such data is to average the electric potentials over trials, yielding what are called event-related potentials (ERPs, Figure 6B). The reliability of these trial-averages is relatively low (Figure 6 B & D show mean and standard-error, and 6 C & E shows single trial data). The mean SNR across all electrodes is $S\sqrt{N} = 0.72$ (Figure 6 A). We are multiplying with \sqrt{N} because, typically, the goal is to determine if the mean value differs significantly from zero, and thus the standard-error of the mean is the relevant quantity.

When we apply CorrCA to these data, we obtain a series of components with high inter-trial correlation (Figure 6 F). CorrCA components were extracted using shrinkage regularization ($\gamma = 0.4$, see Section 8) on a training set of $N = 45$ trials (leaving 1 trial out for testing). Performance was evaluated on the leave-one-out test set. The first three (highlighted in dark blue) are significant at the $\alpha = 0.05$ level according to a non-parametric test based on circularly shifted surrogate data (see Section 9). The first two of these components have an SNR of $S\sqrt{N} = 3.3$ and 1.6. Evidently, component 1 is very reliable (Figure 6 G shows that the mean is several SEM away from the baseline). The deflections are now obvious even in single trials without the need to average (Figure 6 I). The spatial distribution of this component activity (Figure 6 H) is indicative of the well-known ERN. Component 2 (Figure 6 J) is indicative of the readiness potential (Deecke et al., 1969). It rises leading up to the button push at time $t = 0ms$, and has a spatial distribution over parietal and motor areas (Figure 6 K).

Note that CorrCA has reduced the $D = 64$ dimensional data to just a few components that capture the reliable portion of the data (high SNR; Figure 6 F). By compactly representing neural activity in a small number of components, it becomes easier to probe for changes in activity due to manipulation of experimental variables, whose effects on the original $D = 64$ dimensional data may be obscured due to the lower SNR and the multiple comparison problem.

11.5 Effect of regularization on the reliability of EEG responses

Previous work has shown that the inter-subject correlation of EEG responses to popular audiovisual stimuli (i.e., advertisements aired during the Super Bowl) is a strong predictor of the audience’s reception to the stimuli (Dmochowski et al., 2014). Here we employed the data from one of these ads to evaluate the effect of different regularization strategies on the resulting ISC (Section 8). For both the TSVD and shrinkage approaches, we spanned the space of regularization strength (a single parameter, K and γ , in each case) and measured the reliability in each case. The training set was the EEG data from 12 subjects during the first viewing of the ads, while the EEG data collected during the second viewing served as the test set.

The sum of the first 3 inter-subject correlation values (generalized eigenvalues) for both regularization methods followed a similar trajectory with increasing regularization strength (decreasing K and increasing γ ; Figure 7 B & C). On the training data, ISC drops monotonically, whereas on the test data a maximum is achieved at intermediate regularization values. On these data, shrinkage regularization was most effective at $\gamma = 0.4$ and TSVD

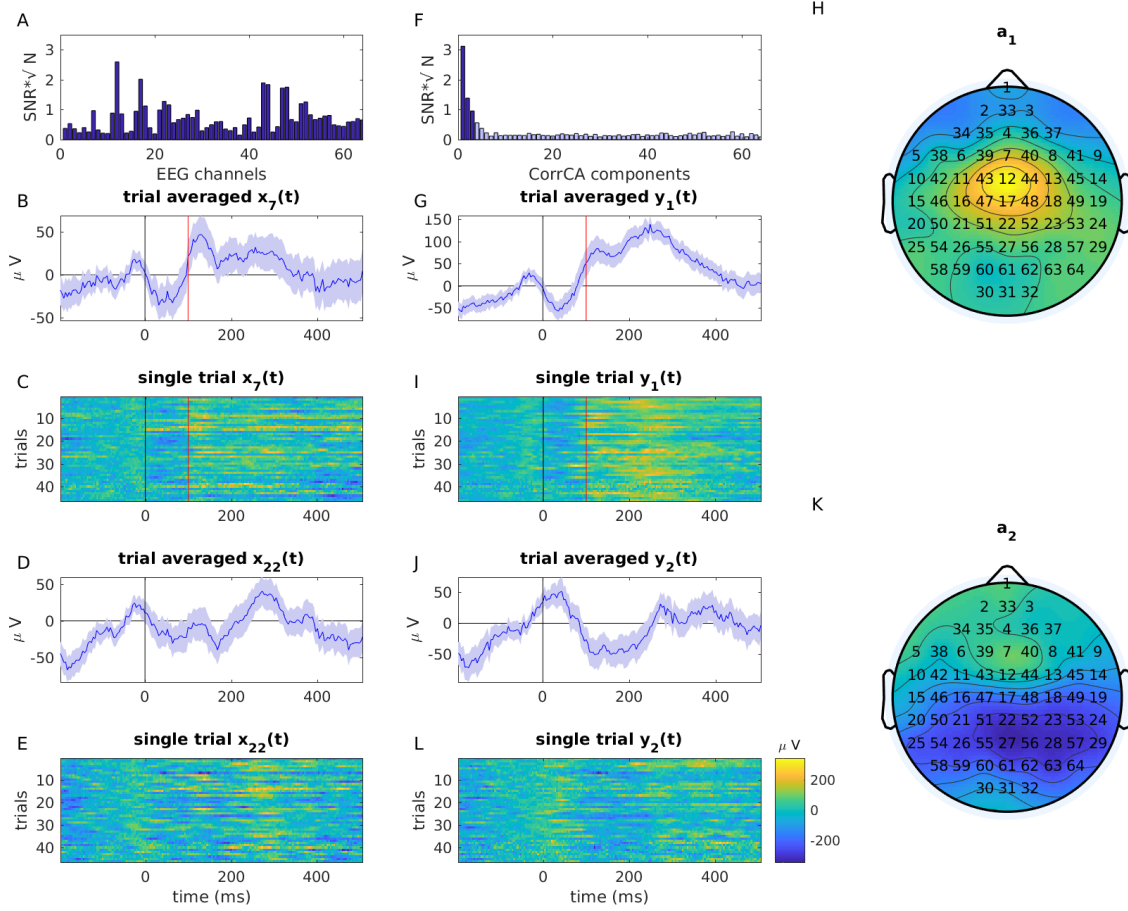


Figure 6: **Event-related potentials.** EEG recordings from a single participant collected during a speed two-alternative forced-choice task (Eriksen Flanker Task). (A-E) Original EEG data $x_j(t)$, highlighting two channels, $j = 7$ (Fz electrode, SNR=0.97) where the “error-related negativity” is expected to be pronounced (between 0 and 100ms; black and red vertical lines), and $j = 22$ (PCz electrode, SNR=1.3) where a “readiness potential” is typically observed. (F-L) First and second correlated components with the strongest inter-trial correlation. (A & F) Signal-to-Noise Ratio computed from the inter-trial correlation (Eq. 25) for original data and extracted components respectively. Dark shaded bars indicate significant components (Circular shuffle statistic on the training set; $\alpha < 0.05$; see Section 9) (B, D, G, F) Average across $N = 46$ repeated trials. Blue-shaded area indicates standard-error of the mean. Evidently the extracted components have a smaller SEM relative to the mean values. The SNR measures is multiplied with \sqrt{N} to parallel the SEM shown here. SNR of 2, for instance, indicates that the mean is 2 SEM away from zero baseline. (C, I, E, F) EEG resolved over all trials to visualize the inter-trial variability. (H & K) Forward model of the two strongest components with distributions consistent with the ERN and readiness potential respectively. Data from Parra et al. (2002).

when retaining $K = 20$ out of a total of $D = 64$ dimensions in the within-subject covariance \mathbf{R}_W .

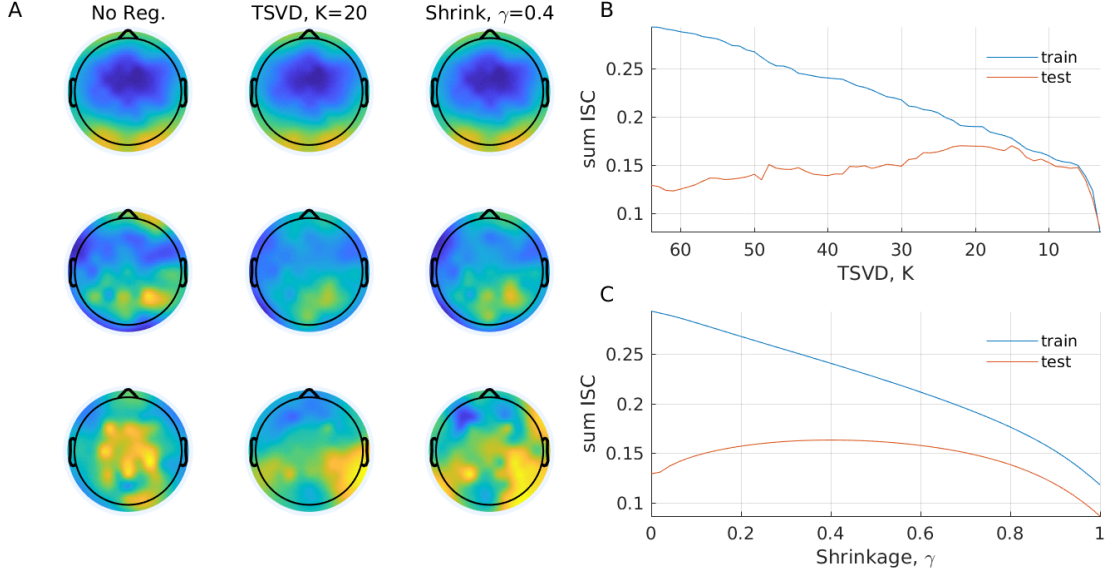


Figure 7: **Regularization increases reliability of EEG test data.** The inter-subject correlations of EEG responses from 12 subjects viewing a popular television advertisement (Dmochowski et al., 2014). We took the data of the highest-scoring advertisement and learned the reliability-maximizing dimensions for varying levels of TSVD and shrinkage regularization. (A) The spatial distributions of the three most correlated components. Note that the distributions of the second and third components were distinct for unregularized, TSVD-regularized and shrinkage-regularized CorrCA. (B) Performance with TSVD as a function of K (decreasing K corresponds to stronger regularization), and (C) performance with shrinkage as a function of γ (increasing γ corresponds to stronger regularization). Components were extracted on the data from a first viewing of the advertisement (training) and evaluated on data from a second viewing (test). Reliability peaks at $\gamma = 0.4$ for shrinkage, and when truncating \mathbf{R}_W to $K = 20$ dimensions, with very similar peak values of ≈ 0.16 (sum of first three inter-subject correlations) for the two regularization approaches.

12. Performance evaluation on simulated data

In this section we will evaluate under which conditions CorrCA identifies the correct directions in space. Additionally, we will compare the accuracy of the statistical tests described in Section 9 at estimating the correct number of components. To this end, we generated artificial data with known properties. The data are generated assuming a known number of correlated components (signals) and additive spatially correlated noise. The following factors were varied parametrically: the number of subjects (raters, repeats), N , the number

of samples per subject, T , the number of dimensions, D , the number of correlated components, K , and the signal-to-noise ratio (SNR) as defined in the space of multivariate measurements. Each simulated correlated components was identically reproduced in each subject, so that the ISC of all components was equal to one. We further varied the temporal dependency structure of the signal and noise components (IID or pink noise), the distribution of the signal and noise components (Gaussian or χ^2 distributed), and the heterogeneity of the signal and noise subspaces (either the same or different for all subjects). Signal components were generated to be correlated across subjects, but uncorrelated with each other. Noise components were uncorrelated with each other as well as across subjects. The number of noise components was fixed to D . The following default parameters were used unless otherwise noted: $N = 5$, $T = 200$, $D = 30$, $K = 10$, SNR = 0 dB, no regularization, IID Gaussian signal and noise components, ISC = 1 for all K components.

12.1 Data generation and evaluation methods

The generated signal and noise components, $\mathbf{s}^l(t) \in \mathbb{R}^K$ and $\mathbf{n}^l(t) \in \mathbb{R}^D$, $t = 1, \dots, T$, $l = 1, \dots, N$, were mapped to the measurement space as $\mathbf{x}_s^l(t) = \mathbf{A}_s^l \mathbf{s}^l(t)$, $\mathbf{x}_n^l(t) = \mathbf{A}_n^l \mathbf{n}^l(t)$ and normalized as $\mathbf{x}_s^l(t) \leftarrow \mathbf{x}_s^l(t) / \|\mathbf{x}_s^l(t)\|_F$, $\mathbf{x}_n^l(t) \leftarrow \mathbf{x}_n^l(t) / \|\mathbf{x}_n^l(t)\|_F$, where $\|\mathbf{x}\|_F$ denotes the Frobenius norm of the multivariate data set $\mathbf{x}(t)$. The mixing matrices $\mathbf{A}_s^l = \mathbf{O}_s^l \mathbf{D}_s^l \in \mathbb{R}^{D \times K}$ and $\mathbf{A}_n^l = \mathbf{O}_n^l \mathbf{D}_n^l \in \mathbb{R}^{D \times D}$ were generated as products of matrices $\mathbf{O}_s^l \in \mathbb{R}^{D \times K}$ ($\mathbf{O}_n^l \in \mathbb{R}^{D \times D}$) with random orthonormal columns and diagonal matrices $\mathbf{D}_s^l \in \mathbb{R}^{K \times K}$ ($\mathbf{D}_n^l \in \mathbb{R}^{D \times D}$), the diagonal entries of which were drawn randomly as $D_{ii} = \exp(d_i)$, $d_i \sim \mathcal{N}(0, 1)$ and normalized to a maximum of 1. This ensured that the non-zero eigenvalues of the signal and noise covariances matrices decayed exponentially as is the case for many real-world data sets. Unless otherwise noted, the same mixing matrices $\mathbf{A}_s^l \equiv \mathbf{A}_s$ and $\mathbf{A}_n^l \equiv \mathbf{A}_n$ were used for all subjects, reflecting the fundamental assumption of CorrCA that the spatial covariance structure of signal and noise components is the same in all subjects. The emulated data were generated as $\mathbf{x}^l(t) = \xi \mathbf{x}_s^l(t) + (1 - \xi) \mathbf{x}_n^l(t)$, where the scalar parameter $\xi = 10^{\text{SNR}/20} / (1 + 10^{\text{SNR}/20})$ was used to adjust the SNR. Note that SNR was defined here in terms of the contribution of the signal and noise components to the Frobenius norm of the entire multivariate measurement. It is, therefore, different from the definition provided in Eqs. (18) and (25), which applies to single channels or components and relates to the ISC through Eq. (22). Note that in most of our experiments, the ISC of each simulated signal component was set to 1, corresponding to infinite SNR according to Eq. (22).

We applied CorrCA to the emulated data and measured its performance in terms of the achieved ISC (average over the first K components) on the training set. We also measured the average ISC for a test set, i.e., using the same CorrCA projections \mathbf{V} on new emulated data of identical size. Moreover, we measured the performance of CorrCA to reconstruct the true (emulated) correlated components $\mathbf{s}^l(t)$ and their corresponding mixing matrices \mathbf{A}_s^l by comparing them to $\mathbf{y}^l(t)$ and the estimated forward model $\hat{\mathbf{A}}$ (Section 10). The performance metric for this was the Pearson correlation between individual simulated and reconstructed components or columns of \mathbf{A}_s . With this, we measure if each component was correctly identified. However, because components with equal ISC can be arbitrarily mixed within a subspace (Appendix A.3), we also assessed identifiability in terms of the angle between the subspaces spanned by the first K columns of the estimated $\hat{\mathbf{A}}$ and \mathbf{A}_n ,

as well as the angle between the simulated components $\mathbf{s}^l(t)$ and the first K dimensions of $\mathbf{y}^l(t)$ reconstructed by CorrCA. Angles were normalized to the interval $[0, 1]$. Finally, we estimated the number of simulated correlated components, K , using phase-scrambled surrogate data, surrogate data obtained using random circular shifts, and the parametric F-test. Empirical null distributions were obtained using 1000 surrogate data sets. The number of components with p-values smaller than $\alpha = 0.05$ was used as an estimate for K . For the parametric test, the T samples were randomly split into training and test sets of equal size, where the CorrCA projections \mathbf{V} were obtained on the training set, and the statistical assessment was conducted on the test set. For this approach, the median number of components with p-values smaller than $\alpha = 0.05$ across 100 random train/test splits was used as an estimate of K .

All experiments were repeated 100 times. Mean values and standard deviations of all performance measures are depicted in Figures 8–11.

12.2 Accuracy as a function of Signal-to-Noise Ratio

Figure 8 depicts CorrCA performance as a function of measurement SNR for fixed $T=200$, $D=30$, $N=5$, $K=10$. SNR values range from -40 dB to 40 dB. It is apparent that average training and test ISC reach the optimal value of 1 for very high SNR. For very low SNR ranges, training ISC significantly exceeds test ISC, indicating over-fitting. The identification of the correlated subspace converges to the optimal value for high SNR. However, individual components are not perfectly identifiable even for high SNR because they share the same ISC values (see Appendix A.3 for a discussion). The identifiability of individual components becomes possible if the ISC of the simulated signal components are adjusted to linearly decrease from 1 down to $1/K$, and if the measurement SNR is high (data not shown). In practice, one should keep in mind that the uniqueness of the ISC (and thereby, their individual identifiability) depends on the amount of noise that is collinear to each original correlated dimension. In the IID case, all estimates of K converge to the true number of 10 for high SNR. Here, the parametric test and the surrogate data approach using random circular shifts perform similarly, while the surrogate data approach using phase scrambling performs considerably worse, presumably due to the absence of a well-defined notion of frequency and phase in the sense of the Fourier transform. In the case of dependent (pink noise) samples, both surrogate data approaches perform identically, converging to the true value of K for high SNR. In contrast, the parametric test, which incorrectly assumes IID data, overestimates the number of correlated components across the entire SNR range, as expected.

12.3 Accuracy of estimating dimensionality of correlated components

The performance of CorrCA as a function of the true number of correlated components, K , is depicted in Figure 9. Here, $T = 200$, $D = 30$, $N = 5$, $\text{SNR} = 0$ dB, where K was varied from 3 to 28. As the overlap between signal and noise subspaces increases with K , the average ISC of the reconstructed correlated components drops. A similar decline is seen in the reconstruction of simulated correlated components and their forward models (data not shown). As a result, the percentage of correlated components that can be recovered (i.e., reach statistical significance) also decreases with increasing K .

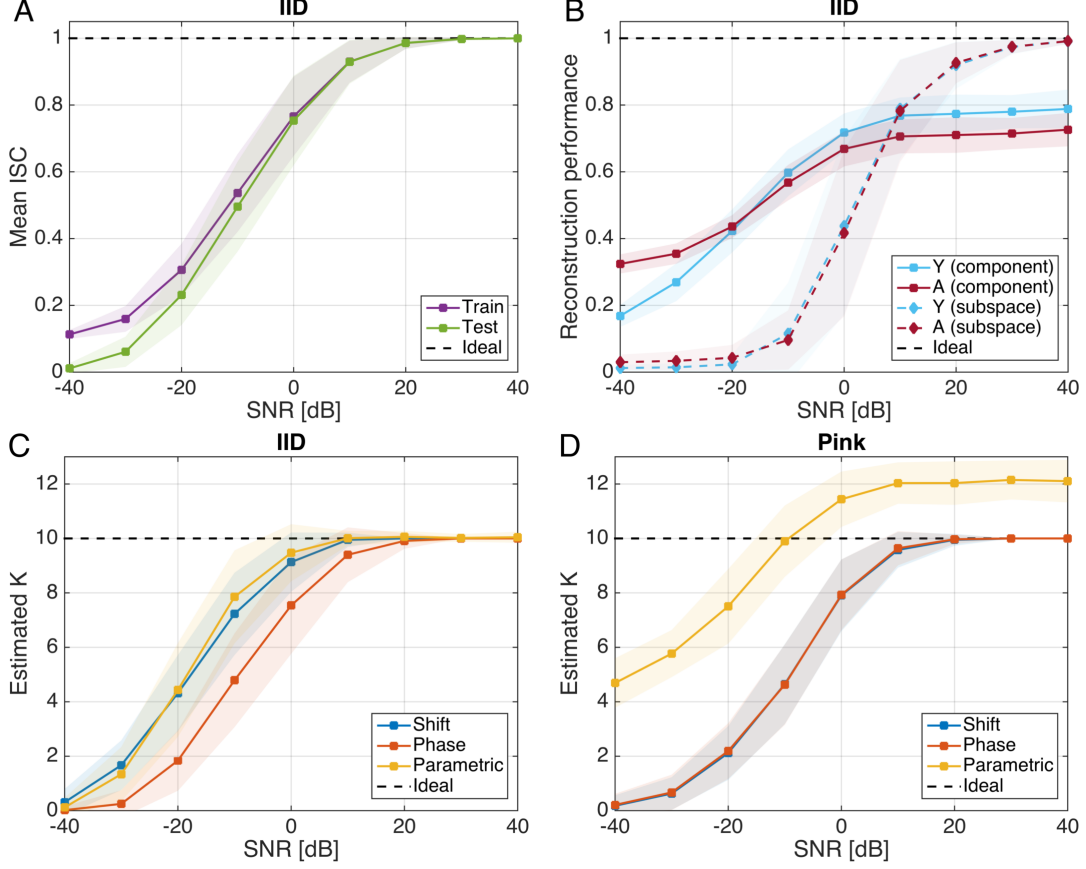


Figure 8: CorrCA performance as a function of signal-to-noise ratio (SNR). Other parameters were fixed to $T = 200$, $D = 30$, $N = 5$, $K = 10$. Plotted are averages across 100 experimental repetitions, while corresponding standard deviations are shown as transparent areas. (A) The average ISC of the reconstructed components converges to the maximal value of 1 for very high SNR. For very low SNR, the expected value of 0 is exceeded on training data, indicating overfitting. (B) CorrCA finds to correct subspace of correlated components if the SNR is sufficiently high. Individual components may, however, not be identifiable if their ISC are too similar. (C) In case of IID data, all statistical tests to estimate K converge to the true number of 10 for high SNR. (D) In case of dependent (pink noise) samples, only surrogate data approaches perform well, while the parametric test overestimates K .

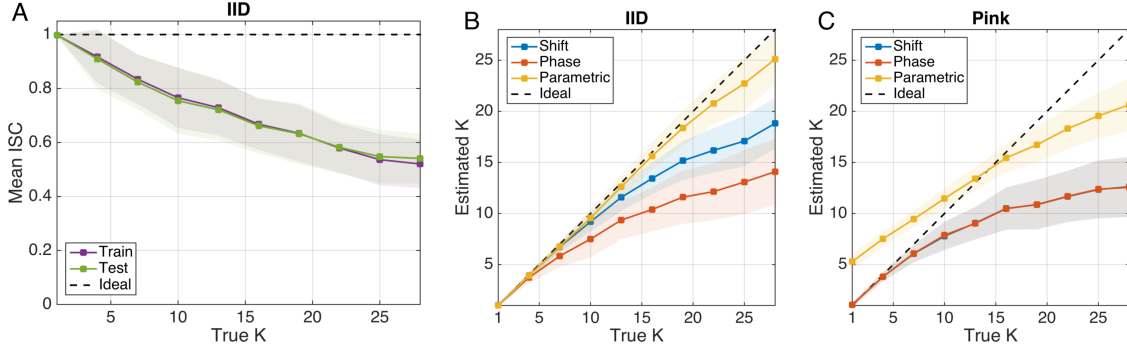


Figure 9: CorrCA performance as a function of the true number of correlated components, K . Other parameters were fixed to $T = 200$, $D = 30$, $N = 5$, $\text{SNR} = 0$ dB. (A) The average ISC of the reconstructed correlated components drops with increasing K . (B) Consequently, the number of correlated components can be less well estimated, the higher K . For IID data, this number is bound from above by the true number for all statistical approaches. (C) Overestimation of K may occur for pink noise data when the parametric F test is used.

Figure 10 shows the estimated number of correlated components as a function of the number of data points, T , and the number of repetitions (subjects/raters), N , with fixed $D = 30$, $K = 10$, $\text{SNR} = 0$ dB. In case of IID data, all estimates converge to the true value of 10 for increasing T or N . This is also true for pink noise data in combination with non-parametric statistical tests. For the parametric test, however, the number of seemingly correlated components diverges as T increases, and is overestimated regardless of N .

12.4 Dependence on signal and noise distributions

Figure 11 A & B shows the performance of CorrCA for different signal and noise distributions. Here, $T = 200$, $D = 30$, $N = 2$, $K = 10$, $\text{SNR} = 0$ dB. Signal and noise components were generated either as Gaussian or squared Gaussian (χ^2 -distributed). For Gaussian distributed components, we considered an additional case, where observations $\mathbf{x}^l(t)$ were dichotomized (thus, Bernoulli distributed) by taking their sign. This simulation scenario resembled the typical setting in which two raters provide a binary assessment of the same issue. While non-Gaussianity of the underlying components does not substantially affect the extraction of correlated components, the same is considerably more difficult in the presence of dichotomous observations. An additional analysis was conducted for IID Gaussian data and $N = 5$ to assess the performance of CorrCA when signal and noise covariance structures (as defined by the mixing matrices \mathbf{A}_s^l and \mathbf{A}_n^l , $n = 1, \dots, N$) differ across subjects (Figure 11 C & D). Significant drops in the number of estimated correlated components as well as the average ISC are observed if the signal covariance, the noise covariance, or both, differ across subjects. This result illustrates that identical covariance structures of signal *and* noise components across subjects are a fundamental assumption of CorrCA. If this assumption is suspected to be violated, the use of multi-set canonical correlation analysis

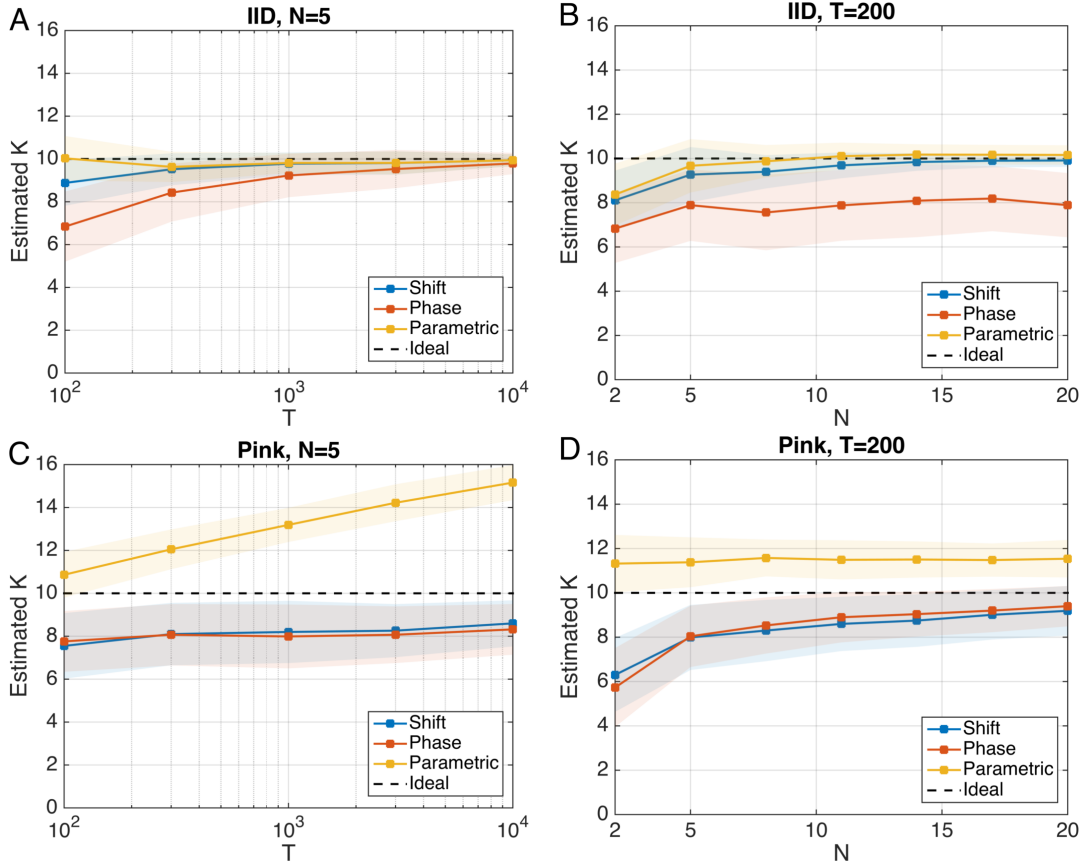


Figure 10: Estimated number of correlated components as a function of the number of data points, T , (left panels), and the number of repetitions (subjects/raters), N , (right panels). Other parameters were fixed to $D = 30$, $K = 10$, $\text{SNR} = 0$ dB. (A & B) In case of IID data, all estimates converge to the true value of 10 for increasing T or N . (C & D) For pink noise data, only non-parametric statistical tests converge to the true value.

(MCCA, which estimates a separate set of projections, \mathbf{V}^l , for each subject, Kettenring, 1971) may be beneficial, or approaches that can gradually move from CorrCA for multi-set CCA (Kamronn et al., 2015).

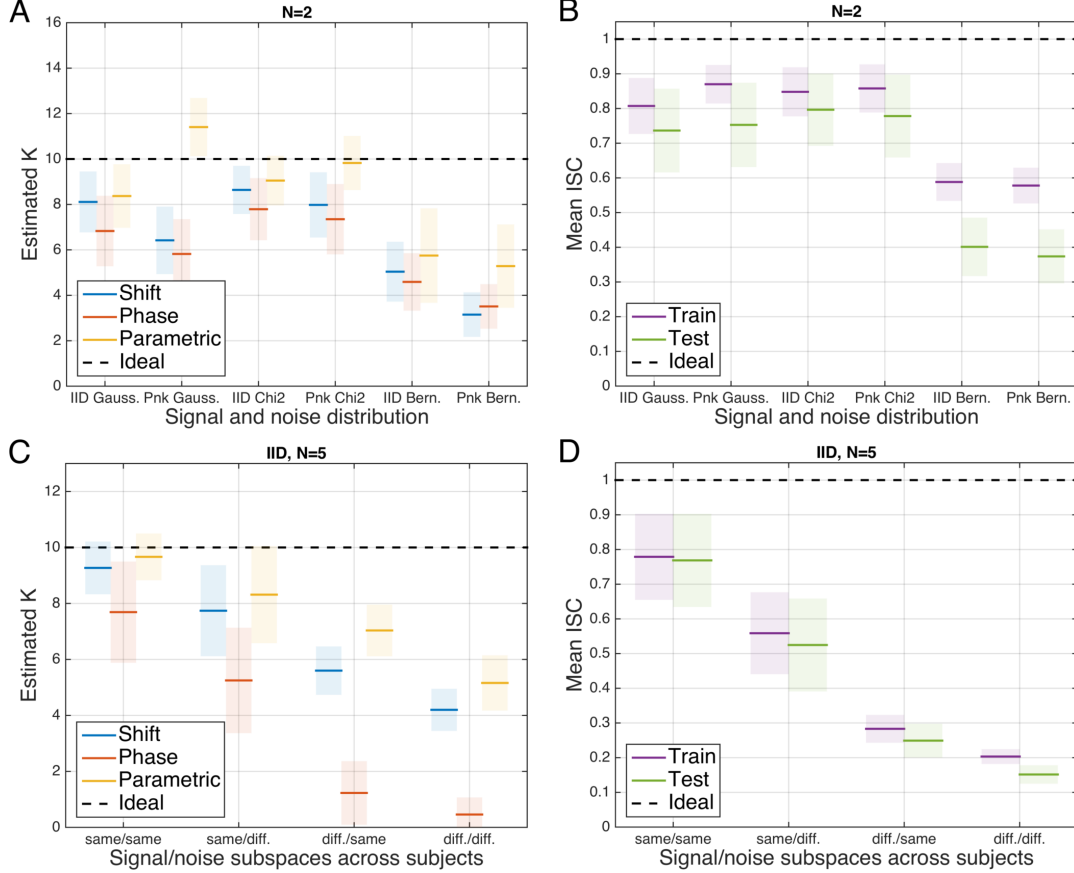


Figure 11: CorrCA performance as a function of signal and noise distributions. Other parameters were fixed to $T = 200$, $D = 30$, $K = 10$, $\text{SNR} = 0$ dB. (A & B) Performance for Gaussian and squared Gaussian (χ^2 -distributed) signal and noise components, as well as for dichotomized (Bernoulli-distributed) observations. Data points were either drawn IID or sampled from a pink noise process. While non-Gaussianity of the underlying components does not substantially affect the extraction of correlated components, the same is considerably more difficult in the presence of dichotomous observations. (C & D) performance on IID Gaussian data when signal and noise covariance structure differs across repetitions (e.g., subjects, raters). Significant drops in the number of estimated correlated components as well as the average ISC are observed if the signal covariance, the noise covariance, or both, differ across subjects.

13. Conclusion

The goal of this work was to provide a formal, yet didactic and comprehensive treatment of this new component analysis technique. The analytic development resulted in a more efficient scheme for computing and maximizing ISC/IRC (Section 4) as well as an extension to non-linear spaces. We also identified the F-statistic as an exact parametric test for statistical significance, which is valid in the case of IID data (Section 9). For the case of non-IID data we demonstrated the effectiveness of circular-shift shuffle statistics as an efficient non-parametric test of significance (Section 12). As a result of these developments, the code we make available at <http://parralab.org/corrca> is significantly faster than previous instantiations (e.g. Cohen and Parra, 2016). All figures presented in this paper can be reproduced with this new code base and associated data. We hope that this analysis and code inspires new uses for CorrCA, including kernel-CorrCA.

Acknowledgments

We are grateful to Valentin Rousson who pointed us to work on inter-class correlation, and Oskar Jenni of the Children University Hospital in Zurich, Switzerland who provided the data from (Rousson et al., 2008), which we reanalyzed here in Figure 4. Similarly, we would like to thank Mike Milhalm for pointing us to the problem of identifying parent/child agreement and Lindsay Alexander for providing access to the Healthy Brain Network data (Alexander et al., 2017) for Figure 5. We also thank Samantha Cohen for providing the data from (Cohen and Parra, 2016) for Figure 3. Samantha as well as Jens Madsen made useful comments on an earlier version of this manuscript.

Appendix A. Generalized eigenvectors for two symmetric matrices

A.1 Joint diagonalization

Here we will review the well-know relationship between the joint diagonalization of two symmetric matrices \mathbf{A} and \mathbf{B} and the eigenvectors of $\mathbf{B}^{-1}\mathbf{A}$. Consider eigenvectors arranged as columns in \mathbf{V} with the corresponding eigenvalues in the diagonal matrix $\mathbf{\Lambda}$:

$$\mathbf{A}\mathbf{V} = \mathbf{B}\mathbf{V}\mathbf{\Lambda}. \quad (47)$$

To find the solution \mathbf{V} for this equation, we can replace the positive definite matrix \mathbf{B} with its Cholesky factorization $\mathbf{B} = \mathbf{L}\mathbf{L}^\top$. Insert this into (47) and left-multiply with \mathbf{L}^{-1} to obtain:

$$(\mathbf{L}^{-1}\mathbf{A}\mathbf{L}^{-\top})(\mathbf{L}^\top\mathbf{V}) = (\mathbf{L}^\top\mathbf{V})\mathbf{\Lambda}, \quad (48)$$

$$\mathbf{M}\mathbf{U} = \mathbf{U}\mathbf{\Lambda}, \quad (49)$$

with $\mathbf{M} = \mathbf{L}^{-1}\mathbf{A}\mathbf{L}^{-\top}$ and $\mathbf{U} = \mathbf{L}^\top\mathbf{V}$. Equation (49) is a conventional eigenvalue equation with the same eigenvalues as (47). It is now easy to see that the corresponding eigenvectors $\mathbf{V} = \mathbf{L}^{-\top}\mathbf{U}$ diagonalize matrix \mathbf{A}

$$\mathbf{V}^\top\mathbf{A}\mathbf{V} = \mathbf{U}\mathbf{L}^{-1}\mathbf{A}\mathbf{L}^{-\top}\mathbf{U} = \mathbf{U}^\top\mathbf{M}\mathbf{U} = \mathbf{\Lambda}. \quad (50)$$

They also diagonalize \mathbf{B} , which we see by left-multiplying (47) with \mathbf{V}^\top and right-multiplying with $\mathbf{\Lambda}^{-1}$. This yields:

$$\mathbf{V}^\top \mathbf{B} \mathbf{V} = \mathbf{V}^\top \mathbf{A} \mathbf{V} \mathbf{\Lambda}^{-1} = \mathbf{I}. \quad (51)$$

Thus, the eigenvectors that solve (47) jointly diagonalize \mathbf{A} and \mathbf{B} . The reverse is also true. A matrix \mathbf{V} that satisfies:

$$\mathbf{V}^\top \mathbf{A} \mathbf{V} = \mathbf{\Lambda}_A \quad (52)$$

$$\mathbf{V}^\top \mathbf{B} \mathbf{V} = \mathbf{\Lambda}_B, \quad (53)$$

where $\mathbf{\Lambda}_A$ and $\mathbf{\Lambda}_B$ are diagonal matrices, also satisfy (47). To see this, solve (53) for \mathbf{V}^\top and substitute this into (52), which yields:

$$\mathbf{\Lambda}_B \mathbf{V}^{-1} \mathbf{B}^{-1} \mathbf{A} \mathbf{V} = \mathbf{\Lambda}_A, \quad (54)$$

and therefore

$$\mathbf{B}^{-1} \mathbf{A} \mathbf{V} = \mathbf{V} \mathbf{\Lambda}_B^{-1} \mathbf{\Lambda}_A, \quad (55)$$

which is the same as the eigenvalue equation (47) with

$$\mathbf{\Lambda} = \mathbf{\Lambda}_B^{-1} \mathbf{\Lambda}_A. \quad (56)$$

A.2 Linear combinations

A matrix \mathbf{V} that simultaneously diagonalizes two matrices \mathbf{A} and \mathbf{B} , as in (52)-(53), will also diagonalize any linear combination of these two matrices (Fukunaga, 2013), because

$$\begin{aligned} \mathbf{V}^\top (\alpha \mathbf{A} + \beta \mathbf{B}) \mathbf{V} &= \alpha \mathbf{V}^\top \mathbf{A} \mathbf{V} + \beta \mathbf{V}^\top \mathbf{B} \mathbf{V} \\ &= \alpha \mathbf{\Lambda}_A + \beta \mathbf{\Lambda}_B, \end{aligned} \quad (57)$$

which is obviously a diagonal matrix. Therefore, the eigenvectors of $\mathbf{A}^{-1} \mathbf{B}$ are also eigenvectors of $(\alpha \mathbf{A} + \beta \mathbf{B})^{-1} (\gamma \mathbf{A} + \delta \mathbf{B})$, assuming vectors $[\alpha, \beta]$ and $[\gamma, \delta]$ are not collinear.

A.3 Identifiability

An additional important observation is that the eigenvectors of (47) are only uniquely defined for unique eigenvalues. If an eigenvalue is degenerate, say with multiplicity K , then the corresponding eigenvectors span a K -dimensional subspace. Any vector within that subspace is a solution to the eigenvalue equation with that eigenvalue. In this space any arbitrary rotation will yield a valid solutions. Thus, when estimating components, it is possible that solutions with close-by ISC are “mixed”. Such components are not uniquely identifiable. One should also note that the sign of any eigenvector is arbitrary. If \mathbf{v}_i is a solution, then so is $-\mathbf{v}_i$. One can always arbitrarily swap the sign of \mathbf{v}_i for any component i , which also reverses the sign of y_i^l and \mathbf{a}_i — the i th column of the forward model \mathbf{A} . Thus, keep in mind that in all figures the sign of individual \mathbf{v}_i and \mathbf{a}_i are arbitrary.

Appendix B. Relationship between Scatter matrices and between- and within-subject covariance matrices

Comparing Eq. (16) to (14) yields:

$$\mathbf{R}_T = N\mathbf{S}_B. \quad (58)$$

One can also relate \mathbf{R}_W to \mathbf{S}_T as follows. Expanding the definition (7) yields (with abbreviated notation for the sums):

$$\begin{aligned} \mathbf{R}_W &= \sum_{il} \mathbf{x}_i^l \mathbf{x}_i^{l\top} - \sum_{il} \mathbf{x}_i^l \bar{\mathbf{x}}_*^{l\top} - \sum_{il} \bar{\mathbf{x}}_*^l \mathbf{x}_i^{l\top} + \sum_{il} \bar{\mathbf{x}}_*^l \bar{\mathbf{x}}_*^{l\top} \\ &= \sum_{il} \mathbf{x}_i^l \mathbf{x}_i^{l\top} - T \sum_l \bar{\mathbf{x}}_*^l \bar{\mathbf{x}}_*^{l\top} \\ &= \sum_{il} \mathbf{x}_i^l \mathbf{x}_i^{l\top} - T \sum_l \bar{\mathbf{x}}_*^l \bar{\mathbf{x}}_*^{l\top} + T \sum_l \bar{\mathbf{x}}_*^{*l} \bar{\mathbf{x}}_*^{*l\top} - T \sum_l \bar{\mathbf{x}}_*^{*l} \bar{\mathbf{x}}_*^{l\top} \\ &= \left(\sum_{il} \mathbf{x}_i^l \mathbf{x}_i^{l\top} + T \sum_l \bar{\mathbf{x}}_*^{*l} \bar{\mathbf{x}}_*^{*l\top} \right) - \left(\sum_{il} \bar{\mathbf{x}}_*^l \bar{\mathbf{x}}_*^{l\top} - T \sum_l \bar{\mathbf{x}}_*^{*l} \bar{\mathbf{x}}_*^{*l\top} \right) \\ &= \sum_{il} (\mathbf{x}_i^l - \bar{\mathbf{x}}_*^l)(\mathbf{x}_i^l - \bar{\mathbf{x}}_*^l)^\top - \sum_{il} (\bar{\mathbf{x}}_*^l - \bar{\mathbf{x}}_*^{*l})(\bar{\mathbf{x}}_*^l - \bar{\mathbf{x}}_*^{*l})^\top \\ &= \mathbf{S}_T - T\mathbf{S}_M. \end{aligned} \quad (59)$$

Matrix \mathbf{S}_M , defined in (21), captures the variance of the mean across subjects and is zero when all subjects have equal mean: $\bar{\mathbf{x}}_*^l = \bar{\mathbf{x}}_*^{*l}$.⁴ With this result, scatter and covariance matrices can be related as follows:

$$\mathbf{S}_B = \frac{1}{N} \mathbf{R}_T = \frac{1}{N} (\mathbf{R}_W + \mathbf{R}_B), \quad (60)$$

$$\begin{aligned} \mathbf{S}_W &= \mathbf{S}_T - \mathbf{S}_B = \mathbf{R}_W + T\mathbf{S}_M - \mathbf{S}_B \\ &= \frac{N-1}{N} \mathbf{R}_W - \frac{1}{N} \mathbf{R}_B + T\mathbf{S}_M. \end{aligned} \quad (61)$$

Appendix C. Further remarks on Inter-Subject Correlation

C.1 Relationship of ISC to Intra-Class Correlation

The definition of inter-subject correlation in the present work is similar to the definition of intra-class correlation (ICC) first introduced by Fisher (1925). Fisher's ICC is referred to as pairwise inter-class correlation and differs from Pearson's correlation coefficient (Donner, 1986). A more modern definition of intra-class correlation, which in the present context

4. For time domain signals, this is often the case as it is customary to subtract the mean value (constant offset) to make the signals zero-mean. For rating data, an unequal mean indicates rater bias, i.e. a rater gives systematically lower/higher ratings than other raters, and it may be advantageous to remove this bias by equalizing all mean values. Note that, when $\mathbf{S}_M = 0$, the present definition of ISC is equivalent to the classic definition of intra-class correlation (ICC, see Appendix B). But in general, this matrix is not zero, which is important when generalizing the approach to non-linear transformations. There, enforcing zero mean in \mathbf{x} does not guarantee zero mean in \mathbf{y} .

Algorithm	Statistic	i=1 ... T	l,k=1 ... N	Reference
CorrCA	inter-subject correlation	samples	subjects	present paper
	Signal-to noise ratio	samples	repeats	present paper
LDA	between class separation	classes	exemplars	(Rao, 1948)
	intra-class correlation	classes	exemplars	(Donner, 1986)
	intra-rater correlation	items	raters	(Rousson et al., 2002)
	intra-familial correlation	families	siblings	(Karlin et al., 1981)

Table 2: Meaning of different indices used in the definitions of various measures of correlation.

would allow for a different number of subjects per sample (i.e. N_i), was introduced by Karlin et al. (1981):

$$r_p = \frac{\sum_{i=1}^T \frac{1}{N_i-1} \sum_{l=1}^{N_i} \sum_{k \neq l}^{N_i} (y_i^l - \bar{y}_*^l)(y_i^k - \bar{y}_*^k)}{\sum_{i=1}^T \sum_{l=1}^{N_i} (y_i^l - \bar{y}_*^l)^2}. \quad (62)$$

The definition of pairwise ICC, r_p , differs from our definition of ISC, ρ , in that it subtracts the total mean \bar{y}_* , whereas we subtract the sample mean of each subject, \bar{y}_*^l . The two are identical in the case of unbiased ratings, i.e. $\mathbf{S}_M = 0$ defined in Eq. (21).

In Table 2 we summarize various uses of these correlation measures. For each case the indices play different roles. In the context of ICC, index i represents different classes whereas l, k are different exemplars of a class. Each class can have a different number of exemplars N_i . In the context of ISC, l, k are subjects and i represent measures taken, perhaps in time. In the case of ratings, l, k are the raters and i are the items being rated. In Karlin et al. (1981), the measure r_p is used to assess intra-familial correlations (correlations between siblings). In this case, k, l indexes the siblings, whereas i enumerates the families. The algorithms listed in Table 2 aim to extract components in multi-dimensional data that maximize the corresponding statistic. Where no algorithm is listed, either CorrCA or LDA could be used.

The definition of ISC/IRC in Eq. (3) can be thought of as a Pearson correlation coefficient, where we concatenate the signals (after subtracting the individual subject/rater means) corresponding to all possible pairs of subjects. In contrast to conventional Pearson correlation, with this symmetric definition (where we include pairs lk as well as kl), the signals of different subjects have to have identical scale in order to achieve perfect ISC/IRC (see Section C.2). In the case of ratings, this means that different raters can only differ in their mean ratings but have to otherwise provide identical deviations from the mean in order to achieve perfect inter-rater correlation. This means that this metric is sensitive to multiplicative bias (i.e. each rater/subject has a different scale). The issue of bias in the context of inter-rater agreement is discussed in more detail by Rousson et al. (2002), who argue that Pearson correlation should be used to assess test-retest reliability to account for learning effects of subjects from one test to the next. If there is an undesirable proportional bias, then one can easily correct for this bias by standardizing the data, i.e. dividing by the standard deviation for each subject/rater in each dimension prior to applying CorrCA.

As we have shown here, maximizing IRC is equivalent to maximizing inter-rater-reliability, where we have defined reliability in Eq. (25) as the variance of the mean over the mean of the variance. For instance, if the rating is the speed of performing a task (as in the application 11.2), this would mean that a 100 millisecond variation across repeats is fairly reliable for a task that takes 5 seconds to complete, but really quite unreliable if the task only takes 0.5 second in average.

It should be noted that, when ratings are on a discrete numerical scale, IRC may not be an appropriate measure of reliability. For instance, a rating on an integer scale of 1, 2, 3, 4, 5, may have an inter-rater variability of ± 1.0 . With the present definition of IRC — ρ in Eq. (3) — this same variability would be considered half as reliable if the mean rating is 4 as compared to a mean of 2. Whether this is desirable or not may depend on the specific ratings statistic. Finally, IRC can only be used meaningfully for ratings that are on a proportional scale. For categorical ratings one should use instead the conventional Cohen’s κ or similar inter-reliability measures.

C.2 ISC is normalized

To our knowledge, the present definition of ρ (3) does not appear in this exact form in the literature, except for our previous work (Cohen and Parra, 2016). Therefore, we take some time here to show that this definition of correlation has indeed a maximal value of 1, and that this occurs only when the all signals are identical across subjects (not just proportional as in Pearson’s correlations), except for a subject-dependent mean, which is permitted.

Without loss of generality, let us assume that all signals are zero mean, $\bar{y}_*^l = 0$. To show that $\rho \leq 1$, we can also demonstrate, equivalently, that the following expression is non-negative:

$$\begin{aligned}
0 &\leq (N-1)r_W - r_B \\
&= (N-1) \sum_l \sum_i (y_i^l)^2 - \sum_l \sum_{k \neq l} \sum_i y_i^l y_i^k \\
&= N \sum_l \sum_i (y_i^l)^2 - \sum_i \left(\sum_l y_i^l \right)^2 = E.
\end{aligned} \tag{63}$$

The last expression is abbreviated as E . To find the y_i^l that minimizes E we find where the gradient is zero and check whether the curvature at that location is non-negative.

$$\begin{aligned}
\frac{\partial E}{\partial y_j^k} &= 2N y_j^k - 2 \sum_i \sum_l y_i^l \sum_l \delta_{ij}^{lk} \\
&= 2N y_j^k - 2 \sum_l y_i^l,
\end{aligned} \tag{64}$$

$$\begin{aligned}
\frac{\partial^2 E}{\partial y_j^k \partial y_j^l} &= 2N \delta_{ji}^{kl} - 2 \sum_n \delta_{ij}^{kn} \\
&= 2\delta_{ij}(N\delta^{kl} - 1).
\end{aligned} \tag{65}$$

Solving for $\partial E / \partial y = 0$ yields an unique solution:

$$y_j^k = \frac{1}{N} \sum_l y_j^l = \bar{y}_j^*. \quad (66)$$

This solution is a linear manifold, as one can pick arbitrary scale for \bar{y}_j^* . Inserting this into (63) yields $E = 0$ at that point. To determine whether this is indeed a minimum value for E , and hence $\rho \leq 1$, we need to show that the Jacobian (65) has only non-negative eigenvalues. Because of the δ_{ij} in (65), we can find the eigenvalues for each ij separately, i.e. the eigenvalues of $J = N\mathbf{I} - \mathbf{1}\mathbf{1}^\top$, where \mathbf{I} is the N -dimensional identity matrix and $\mathbf{1}$ is a N -dimensional vector with all values set to 1. This \mathbf{J} is the same for all ij , and the eigenvalue equation is for $\mathbf{y} \in \mathbb{R}^N$:

$$\mathbf{J}\mathbf{y} = \lambda\mathbf{y}. \quad (67)$$

The characteristic polynomial for these eigenvalues reads:

$$\begin{aligned} 0 &= \det(N\mathbf{I} - \mathbf{1}\mathbf{1}^\top - \lambda\mathbf{I}) \\ &= (N - \lambda)^N \det(\mathbf{I} - (N - \lambda)^{-1}\mathbf{1}\mathbf{1}^\top) \\ &= (N - \lambda)^N (1 - (N - \lambda)^{-1}N) \\ &= -(N - \lambda)^{N-1}\lambda. \end{aligned} \quad (68)$$

This means that there is a $(N - 1)$ -fold eigenvalue, $\lambda = N$, and a unique eigenvalue, $\lambda = 0$. Therefore, the Jacobian is semidefinite, i.e. it has positive curvature in all directions, except in the direction of the eigenvectors of $\lambda = 0$. Inserting this in (67) yields $\mathbf{y} = c\mathbf{1}$ with a free parameter c . If we compare that to (66), we see that these are the same, with $c = y_i^*$. This means that, when all signals are the same for all subjects, then we achieve a global minimum for E and, therefore, ρ is maximal and equals to 1. The curvature is zero in one direction at the minimum because one can change the global scale of all signals without changing $E = 0$.

C.3 ISC between individuals and a group of subjects

In a number of studies, we compare brain responses of individual subjects to that of the group by correlating between pairs of subjects, and then averaging over pairs involving the subjects of interest. This correlation of individual subject with a group is then used to compare with individual measures (Ki et al., 2016; Cohen and Parra, 2016; Petroni et al., 2018). For this purpose, we used the following definition for single-subject ISC (Cohen and Parra, 2016):

$$\rho_k = \frac{\sum_{l=1}^N \sum_{N=1, l \neq k}^N (r_{kl} + r_{lk})}{\sum_{l=1}^N \sum_{N=1, l \neq k}^N (r_{ll} + r_{kk})}, \quad (69)$$

$$r_{kl} = \sum_{i=1}^T (y_i^k - \bar{y}_*^k)(y_i^l - \bar{y}_*^l). \quad (70)$$

This can be computed for each extracted component $y_j(t) = \mathbf{v}_j^\top \mathbf{x}(t)$.

References

- Lindsay M. Alexander, Jasmine Escalera, Lei Ai, Charissa Andreotti, Karina Febre, Alex Mangone, Natan Vega Potler, Nicolas Langer, Alexis Alexander, Meagan Kovacs, Shannon Litke, Bridget O’Hagan, Jennifer Andersen, Batya Bronstein, Anastasia Bui, Mari-jayne Bushey, Henry Butler, Victoria Castagna, Nicolas Camacho, Elisha Chan, Danielle Citera, Jon Clucas, Samantha Cohen, Sarah Dufek, Megan Eaves, Brian Fradera, Judith Gardner, Natalie Grant-Villegas, Gabriella Green, Camille Gregory, Emily Hart, Megan Horton, Shana Harris, Catherine Lord, Danielle Kahn, Katherine Kabotyanski, Bernard Karmel, Simon P Kelly, Kayla Kleinman, Bonhwang Koo, Eliza Kramer, Elizabeth Lennon, Ginny Mantello, Amy Margolis, Kathleen Merikangas, Judith Milham, Giuseppe Minniti, Rebecca Neuhaus, Alexandra Nussbaum, Yael Osman, Lucas C. Parra, Ken R. Pugh, Amy Racanello, Anita Restrepo, Tian Saltzman, Batya Septimus, Russ Tobe, Rachel Waltz, Anna Williams, Anna Yeo, F. Xavier Castellanos, Arno Klein, Tomas Paus, Bennett L. Leventhal, Cameron Craddock, Harold S. Koplewicz, and Michael P. Milham. Data descriptor: An open resource for transdiagnostic research in pediatric mental health and learning disorders. *Scientific Data*, 2017.
- Gaston Baudat and Fatiha Anouar. Generalized discriminant analysis using a kernel approach. *Neural computation*, 12(10):2385–2404, 2000.
- Samantha Cohen, Lucas C. Parra, and Jacek P. Dmochowski. The utility of reliability in decoding neural responses. *bioRxiv*, 2017a.
- Samantha S Cohen and Lucas C Parra. Memorable audiovisual narratives synchronize sensory and supramodal neural responses. *eneuro*, 3(6):ENEURO–0203, 2016.
- Samantha S Cohen, Simon Henin, and Lucas C Parra. Engaging narratives evoke similar neural activity and lead to similar time perception. *Scientific Reports*, 7:4578, 2017b.
- Alain de Cheveigné and Lucas C Parra. Joint decorrelation, a versatile tool for multichannel data analysis. *Neuroimage*, 98:487–505, 2014.
- Lüder Deecke, Peter Scheid, and Hans H Kornhuber. Distribution of readiness potential, pre-motion positivity, and motor potential of the human cerebral cortex preceding voluntary finger movements. *Experimental Brain Research*, 7(2):158–168, 1969.
- Jacek P Dmochowski and Anthony M Norcia. Cortical components of reaction-time during perceptual decisions in humans. *PloS one*, 10(11):e0143339, 2015.
- Jacek P Dmochowski, Paul Sajda, Joao Dias, and Lucas C Parra. Correlated components of ongoing eeg point to emotionally laden attention—a possible marker of engagement? *Frontiers in human neuroscience*, 6, 2012.
- Jacek P Dmochowski, Matthew A Bezdek, Brian P Abelson, John S Johnson, Eric H Schumacher, and Lucas C Parra. Audience preferences are predicted by temporal reliability of neural processing. *Nature communications*, 5, 2014.
- Jacek P Dmochowski, Alex S Greaves, and Anthony M Norcia. Maximally reliable spatial filtering of steady state visual evoked potentials. *Neuroimage*, 109:63–72, 2015.

- Allan Donner. A review of inference procedures for the intraclass correlation coefficient in the one-way random effects model. *International Statistical Review/Revue Internationale de Statistique*, pages 67–82, 1986.
- Richard O Duda, Peter E Hart, and David G Stork. *Pattern classification*. John Wiley & Sons, 2012.
- Ronald A Fisher. The use of multiple measurements in taxonomic problems. *Annals of human genetics*, 7(2):179–188, 1936.
- Ronald Aylmer Fisher. *Statistical methods for research workers*. Oliver and Boyd, 1925.
- Keinosuke Fukunaga. *Introduction to statistical pattern recognition*. Academic press, 2013.
- Per Christian Hansen. Regularization tools: A matlab package for analysis and solution of discrete ill-posed problems. *Numerical algorithms*, 6(1):1–35, 1994.
- Stefan Haufe, Frank Meinecke, Kai Gorgen, Sven Dhne, John-Dylan Haynes, Benjamin Blankertz, and Felix Biemann. On the interpretation of weight vectors of linear models in multivariate neuroimaging. *Neuroimage*, 87:96–110, 2014.
- Stefan Haufe, Paul DeGuzman, Simon Henin, Michael Arcaro, Christopher J. Honey, Uri Hasson, and Lucas C. Parra. Elucidating relations between fmri, ecog and eeg through a common natural stimulus. *bioRxiv*, 2017. doi: 10.1101/207456.
- Harold Hotelling. Analysis of a complex of statistical variables into principal components. *Journal of educational psychology*, 24(6):417, 1933.
- Harold Hotelling. Relations between two sets of variates. *Biometrika*, 28(3/4):321–377, 1936.
- Ivan Iotzov, Brian C Fidali, Agustin Petroni, Mary M Conte, Nicholas D Schiff, and Lucas C Parra. Divergent neural responses to narrative speech in disorders of consciousness. *Analns of Clinical and Translational Neurology*, 2017.
- Simon Kamronn, Andreas Trier Poulsen, and Lars Kai Hansen. Multiview bayesian correlated component analysis. *Neural Computation*, 27(10):2207–2230, 2015.
- Samuel Karlin, Edward C Cameron, and Paul T Williams. Sibling and parent–offspring correlation estimation with variable family size. *Proceedings of the National Academy of Sciences*, 78(5):2664–2668, 1981.
- Jon R Kettenring. Canonical analysis of several sets of variables. *Biometrika*, 58(3):433–451, 1971.
- Jason J Ki, Simon P Kelly, and Lucas C Parra. Attention strongly modulates reliability of neural responses to naturalistic narrative stimuli. *The Journal of Neuroscience*, 36(10): 3092–3101, 2016.
- Pei Ling Lai and Colin Fyfe. Kernel and nonlinear canonical correlation analysis. *International Journal of Neural Systems*, 10(05):365–377, 2000.

- Olivier Ledoit and Michael Wolf. A well-conditioned estimator for large-dimensional covariance matrices. *Journal of multivariate analysis*, 88(2):365–411, 2004.
- Scott Makeig, Anthony J Bell, Tzyy-Ping Jung, and Terrence J Sejnowski. Independent component analysis of electroencephalographic data. In *Advances in neural information processing systems*, pages 145–151, 1996.
- Christoph M Michel, Micah M Murray, Göran Lantz, Sara Gonzalez, Laurent Spinelli, and Rolando Grave de Peralta. Eeg source imaging. *Clinical neurophysiology*, 115(10):2195–2222, 2004.
- Sebastian Mika, Gunnar Ratsch, Jason Weston, Bernhard Scholkopf, and Klaus-Robert Mullers. Fisher discriminant analysis with kernels. In *Neural Networks for Signal Processing IX, 1999. Proceedings of the 1999 IEEE Signal Processing Society Workshop.*, pages 41–48. IEEE, 1999.
- Athanasios Papoulis and S Unnikrishna Pillai. *Probability, random variables, and stochastic processes*. Tata McGraw-Hill Education, 2002.
- Lucas Parra, Chris Alvino, Akaysha Tang, Barak Pearlmutter, Nick Yeung, Allen Osman, and Paul Sajda. Linear spatial integration for single-trial detection in encephalography. *NeuroImage*, 17(1):223–230, 2002.
- Lucas C Parra, Clay D Spence, Adam D Gerson, and Paul Sajda. Recipes for the linear analysis of eeg. *Neuroimage*, 28(2):326–341, 2005.
- Agustin Petroni, Samantha S Cohen, Lei Ai, Nicolas Langer, Simon Henin, Tamara Vanderwal, Michael P Milham, and Lucas C Parra. The variability of neural responses to naturalistic videos change with age and sex. *eNeuro*, pages ENEURO–0244, 2018.
- Andreas Trier Poulsen, Simon Kamronn, Jacek Dmochowski, Lucas C Parra, and Lars Kai Hansen. Eeg in the classroom: Synchronised neural recordings during video presentation. *Scientific Reports*, 7:43916, 2017.
- Dean Prichard and James Theiler. Generating surrogate data for time series with several simultaneously measured variables. *Physical review letters*, 73(7):951, 1994.
- C Radhakrishna Rao. The utilization of multiple measurements in problems of biological classification. *Journal of the Royal Statistical Society. Series B (Methodological)*, 10(2):159–203, 1948.
- Valentin Rousson, Theo Gasser, and Burkhardt Seifert. Assessing intrarater, interrater and test–retest reliability of continuous measurements. *Statistics in medicine*, 21(22):3431–3446, 2002.
- Valentin Rousson, Theo Gasser, Jon Caffisch, and Remo Largo. Reliability of the zurich neuromotor assessment. *The Clinical Neuropsychologist*, 22(1):60–72, 2008.
- Jaakko Särelä and Harri Valpola. Denoising source separation. *Journal of machine learning research*, 6(Mar):233–272, 2005.

- Natalie Schaworonkow, Duncan AJ Blythe, Jewgeni Kegeles, Gabriel Curio, and Vadim V Nikulin. Power-law dynamics in neuronal and behavioral data introduce spurious correlations. *Human brain mapping*, 36(8):2901–2914, 2015.
- Bernhard Schölkopf, Alexander Smola, and Klaus-Robert Müller. Nonlinear component analysis as a kernel eigenvalue problem. *Neural computation*, 10(5):1299–1319, 1998.
- Hirokazu Tanaka, Takusige Katura, and Hiroki Sato. Task-related component analysis for functional neuroimaging and application to near-infrared spectroscopy data. *Neuroimage*, 64:308–327, 2013.
- James Theiler, Stephen Eubank, André Longtin, Bryan Galdrikian, and J Doyne Farmer. Testing for nonlinearity in time series: the method of surrogate data. *Physica D: Non-linear Phenomena*, 58(1-4):77–94, 1992.
- Nick Yeung, Matthew M Botvinick, and Jonathan D Cohen. The neural basis of error detection: conflict monitoring and the error-related negativity. *Psychological review*, 111(4):931, 2004.
- Jianguo Zhang, Kai-kuang Ma, et al. Kernel fisher discriminant for texture classification. 2004.